Annexes

Annexe A

Article *Herrmann et al. 2010*, Journal of Geophysical Research

JOURNAL OF GEOPHYSICAL RESEARCH, VOL. 115, C12051, doi:10.1029/2010JC006162, 2010

What induced the exceptional 2005 convection event in the northwestern Mediterranean basin? Answers from a modeling study

Marine Herrmann,[1] Florence Sevault,[1] Jonathan Beuvier,[1,2] and Samuel Somot[1]

Received 1 February 2010; revised 7 October 2010; accepted 15 October 2010; published 21 December 2010.

[1] Open-sea convection occurring in the northwestern Mediterranean basin (NWMED) is at the origin of the formation of Western Mediterranean Deep Water (WMDW), one of the main Mediterranean water masses. During winter 2004–2005, a spectacular convection event occurred, observed by several experimental oceanographers. It was associated with an exceptionally large convection area and unusually warm and salty WMDW. Explanations were proposed tentatively, relating the unusual characteristics of this event to the Eastern Mediterranean Transient (EMT) or to the atmospheric conditions during winter 2004–2005 in the NWMED. They could, however, not be supported until now. Here we used numerical modeling to understand what drove this convection event. The control simulation performed for the period 1961–2006 reproduces correctly the long-term evolution of the Mediterranean Sea circulation, the EMT, and the NWMED convection event of 2004–2005. Sensitivity simulations are then performed to assess the respective contributions of atmospheric and oceanic conditions to this event. The weakness of the winter buoyancy loss since 1988 in the NWMED prevented strong convection to occur during the 1990s, enabling heat and salt contents to increase in this region. This resulted in the change of WMDW characteristics observed in 2005. The strong buoyancy loss of winter 2004–2005 was responsible for the intensity of the convection observed this winter in terms of depth and volume of newly formed WMDW. The EMT did not fundamentally modify the convection process but potentially doubled this volume by inducing a deepening of the heat and salt maximum that weakened the preconvection stratification.

Citation: Herrmann, M., F. Sevault, J. Beuvier, and S. Somot (2010), What induced the exceptional 2005 convection event in the northwestern Mediterranean basin? Answers from a modeling study, *J. Geophys. Res.*, *115*, C12051, doi:10.1029/2010JC006162.

1. Introduction

[2] Open-sea deep convection takes place in a few regions of the world, among which the northwestern Mediterranean basin (NWMED) [*Marshall and Schott*, 1999]. In this region, strong winter surface buoyancy loss associated with northern wind events (Mistral, Tramontane) induce deep convection events, at the origin of the formation of Western Mediterranean Deep Water (WMDW). During winter 2004–2005, an exceptionally strong convection event was observed by several experimental oceanographers [*López-Jurado et al.*, 2005; *Salat et al.*, 2006; *Schröder et al.*, 2006; *Font et al.*, 2007; *Schroeder et al.*, 2008; *Smith et al.*, 2008]: convection reached the bottom and covered an area much larger than usually, and WMDW formed this winter was significantly saltier and warmer than the values reported in the literature (Table 1). Two major explanations for the exceptional characteristics of this convection event (intensity and WMDW characteristics) were proposed by those authors.

[3] First, winter 2004–2005 was one of the coldest and driest winters of the last 40 years [*López-Jurado et al.*, 2005; *Font et al.*, 2007], thus associated with strong surface heat, water and buoyancy losses. The formation of dense water at the surface being triggered by the buoyancy loss, those atmospheric conditions certainly played a role in the intensity of the deep convection event. Moreover, the strong water loss must have induced an increase of the surface salinity which could partly explain the larger salinity of WMDW formed this year.

[4] Second, *López-Jurado et al.* [2005] suggested that the unusual characteristics of the 2005 convection event could be due to an alteration of the water masses advected into the convection area. *Millot* [2005] also proposed that some observed changes in the Western Mediterranean Deep Water masses could be due to the presence of modified eastern waters brought to the Western basin after the Eastern Mediterranean Transient (EMT, corresponding to the shift of production of Eastern Mediterranean Deep Water from the Adriatic to the Aegean subbasins at the beginning of the

[1]CNRM-GAME, Météo-France/CNRS, Toulouse, France.
[2]ENSTA-ParisTech/UME, Palaiseau, France.

0148-0227/10/2010JC006162

Table 1. Observed Characteristics of the Old WMDW (Formed Before 2005) and New WMDW (Formed in 2005)[a]

Authors	Old DW			New DW		
	T_{DW} (°C)	S_{DW}	ρ_{DW} (kg m^{-3})	T_{DW} (°C)	S_{DW}	ρ_{DW} (kg m^{-3})
Mertens and Schott [1998]	12.75–12.92	38.41–38.46	29.09–29.10			
López-Jurado et al. [2005]	12.83–12.85	38.44–38.46		12.88	38.48–38.49	
Schröder et al. [2006]	12.8–12.85	38.44–38.46		12.87–12.90	38.47–38.48	
Salat et al. [2006]	12.75–12.82	38.43–38.47	29.115–29.120	12.87–12.90	38.49–38.50	29.130
Font et al. [2007]	12.8–12.9	38.43–38.46	29.09–29.10	12.88	38.48	29.117
Smith et al. [2008]	12.86	38.46	29.108	12.89	38.48	29.113
This study:CTRL, 2005	12.73–12.80	38.423–38.44	>29.10	12.90	38.483	29.116

[a]The values obtained in CTRL from the temperature-salinity diagram shown in Figure 7a are also indicated, with old WMDW corresponding to water denser than 29.10 kg m^{-3} present in LION on 1 December 2004 and new WMDW corresponding to the densest water formed on 10 March 2005. T_{DW}, temperature; S_{DW}, salinity; ρ_{DW}, density.

1990s; see *Roether et al.* [2007] for a detailed description of the EMT). *Gasparini et al.* [2005] indeed showed that the EMT induced an increase of the density of the eastern waters flowing westward through the Sicily channel associated with a remarkable injection of heat and salt in the deep Tyrrhenian subbasin. Consequently, *López-Jurado et al.* [2005], *Schröder et al.* [2006] and *Schroeder et al.* [2008] suggested that the EMT induced the warming and salting of the intermediate and deep layer of the NWMED. Being mixed with the rest of the water column when deep convection occurs, this layer participates in the composition of WMDW. This could thus explain the warming and salting of WMDW formed in 2005. Moreover, it could have induced a modification of the water column structure, hence of the stratification, which could have impacted the extension of the deep convection volume.

[5] Until now, those explanations were proposed tentatively, but have not been supported yet. In particular, the relative contributions of the atmospheric and oceanic conditions to the characteristics of the 2005 deep convection event still need to be clearly quantified. Observations were indeed very useful to characterize this event, but they do not provide sufficiently continuous spatial and temporal coverage to answer to those questions. Realistic numerical modeling can help to apprehend the 4-D evolution of the sea and therefore help to interpret and understand observations. To our knowledge, however, no realistic oceanic simulation of the NWMED circulation in 2004–2005 has been performed until now: *Herrmann et al.* [2009] presented a simulation that was carried out for the 1998–2007 period, but it did not reproduced the change of WMDW characteristics observed in 2005. In this context, our goal is to perform realistic numerical modeling of the NWMED 2005 convection event but also of the long-term Mediterranean circulation before 2004, in order to understand precisely what triggered this event, and to quantify the contribution of the different factors involved.

[6] We present the numerical model and the simulations in section 2. Results are then presented and discussed in section 3. We first examine the long-term evolution of the water column until 2004 in the NWMED and the influence of the EMT on the NWMED oceanic conditions. We then show that the model is able to represent realistically the 2004–2005 NWMED convection event. Finally, we determine which factors were responsible for the exceptional characteristics of this event. For that, we assess the influence of the oceanic and atmospheric conditions before and during winter 2004–2005. Conclusion and future works are presented in section 4. Note that in the following, all the values given for temperature and density correspond to potential temperature and density.

2. Tools and Methods

2.1. Numerical Model

[7] We use the NEMOMED8 model, a Mediterranean version of the NEMO numerical ocean model [*Madec*, 2008] used and described by *Beuvier et al.* [2010] and *Sevault et al.* [2009]. It is an updated version of the model used by *Somot et al.* [2006] and *Herrmann et al.* [2008] to study the NWMED deep convection. NEMOMED8 covers the whole Mediterranean Sea plus a buffer zone including a part of the near Atlantic Ocean (see Figure 1). The horizontal resolution is 1/8° × 1/8° cos(ϕ), with ϕ the latitude, equivalent to a range of 9 to 12 km from the north to the south of the Mediterranean domain. The grid is tilted and stretched at the Gibraltar Strait in order to better follow the SW-NE axis of the real strait and to increase the local resolution up to 6 km. The Gibraltar Strait is represented with a two-grid point wide strait. NEMOMED8 has 43 vertical Z levels with an inhomogeneous distribution (from Z = 6 m at the surface to Z = 200 m at the bottom with 25 levels in the first 1000 m). The bathymetry is based on the ETOPO 5′ × 5′ database [*Smith and Sandwell*, 1997]. A time step of 20 min is applied. NEMOMED8 has a filtered free-surface and partial-cell parametrization. The horizontal eddy diffusivity is fixed to 125 m^2 s^{-1} for the tracers (temperature, salinity) using a Laplacian operator and the horizontal viscosity coefficients is fixed to −1.0 10^{10} m^2 s^{-2} for the dynamics (velocity) using a biharmonic operator. A 1.5 turbulent closure scheme is used for the vertical eddy diffusivity [*Blanke and Delecluse*, 1993] with an enhancement of the vertical diffusivity coefficient up to 50 m^2 s^{-1} in case of unstable stratification. A no-slip lateral boundary condition is used and the bottom friction is quadratic. The TVD (Total Variance Dissipation) scheme [*Barnier et al.*, 2006] is used for the tracer advection. NEMOMED8 conserves energy and enstrophy. The solar radiation can penetrate into the ocean surface layers [*Bozec et al.*, 2008].

2.2. Forcings

2.2.1. Surface Boundary Conditions: Atmospheric Forcing

[8] To prescribe air-sea fluxes to the ocean model, we use the results of a high-resolution atmospheric data set named ARPERA obtained by performing a dynamical downscaling of ECMWF fields. Based on the study of the real case of

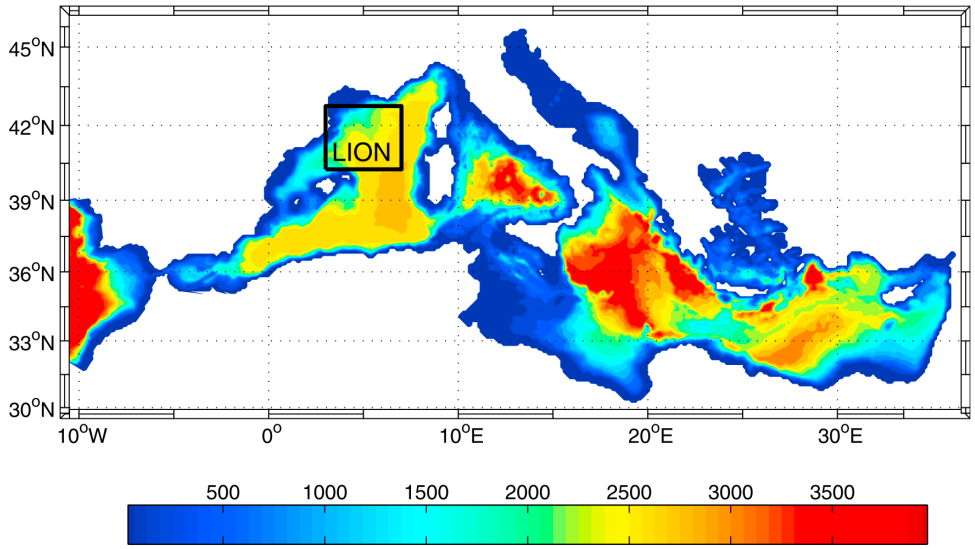

Figure 1. Bathymetry of the modeled domain. The black box corresponds to the LION area, from 3°W to 7°W and from 40.25°N to 42.75°N. Unit is meters.

winter 1986–1987, *Herrmann and Somot* [2008] showed that this data set followed very well the real atmospheric chronology and was relevant to model realistically deep convection in the NWMED. The downscaling method was described in detail by *Guldberg et al.* [2005]. The principle is to use a high-resolution atmospheric model, here ARPEGE-Climate [*Déqué and Piedelievre*, 1995], in which small scales can develop freely and large scales are driven by ECMWF fields. The synoptic chronology then follows that of ECMWF fields while the high-resolution structures of the atmospheric flow are created by the model. For the period 1958–2001, fields of ERA40 reanalysis [*Gibson et al.*, 1997] are used to drive ARPEGE-Climate. Between 2002 and 2006, fields of ECMWF analysis are used, their resolution (0.5° ~ 55 km) being downgraded down to ERA40 resolution (1.125° ~ 125 km) in order to insure consistency between the 1958–2001 and 2002–2006 periods.

[9] The forcing fields for NEMOMED8 are the momentum, freshwater and heat fluxes. A relaxation term toward ERA40 sea surface temperature (SST) is applied for the heat flux. This term actually plays the role of a first-order coupling between the SST computed by the ocean model and the atmospheric heat flux, ensuring the consistency between those terms. Following *CLIPPER Project Team* [1999], the relaxation coefficient is −40 W m^{-2} K^{-1}, equivalent to an 8 day restoring time scale.

[10] The LION area (see Figure 1) is chosen in order to cover entirely the region of NWMED deep convection reported in the literature [*Marshall and Schott*, 1999]. Figure 2 shows the evolution of the mean September–November, December–February and September–February surface heat, water and buoyancy losses over LION (*HL*, *WL* and *BL*) between winters 1961–1962 and 2005–2006. The following formula [*Mertens and Schott*, 1998] is used for *BL*:

$$BL = g.\left(\frac{\alpha.HL}{\rho_0.C_p} - \beta.SSS.WL\right) = BL_H + BL_W \qquad (1)$$

where g = 9.81 m s^{-2} is the gravitational acceleration, ρ_0 = 1020 kg m^{-3} is the density reference, C_p = 4000 J kg^{-1} K^{-1} is the specific heat of water, $\alpha = 2.10^{-4}$ K^{-1} and $\beta = 7.6.10^{-4}$ are the thermal and saline expansion coefficients and *SSS* is the sea surface salinity. In agreement with what was previously observed by *López-Jurado et al.* [2005] using NCEP [*Kalnay et al.*, 1996] and by *Font et al.* [2007] using the data of the Portbou station from the Catalan Meteorological service, the ARPERA data set shows that winter 2004–2005 was the coldest and second driest winter of the 1961–2006 period, hence the one with the strongest buoyancy loss (highest values of *HL* = 265 W m^{-2} versus 147 ± 47 W m^{-2} in average over the 1961–2006 period, *WL* = 4.42 mm d^{-1} versus 2.96 ± 0.79 mm d^{-1} and *BL* = 1.42 10^{-7} m^2 s^{-3} versus 0.80 ± 0.24 10^{-7} m^2 s^{-3}). This was due to the occurrence of several intense atmospheric events associated with strong winds and to cold and dry air masses, during which *HL* and *WL* exceeded 500 W m^{-2} and 10 mm d^{-1}, respectively. This is shown in Figure 3a where we present the evolution of the daily average over LION between December 2004 and April 2005 of *HL*, *WL*, *BL* and the wind velocity computed in ARPERA and of the wind velocity given by QuikSCAT LEVEL 3 data set [*Perry*, 2001] (available on http://podaac.jpl.nasa.gov:2031/DATASET_DOCSqscat_l3.html). Events of strong buoyancy loss are highlighted in gray in Figure 3. As already shown by *Herrmann and Somot* [2008] for winter 1986–1987, ARPERA follows very well the real atmospheric chronology for winter 2004–2005: the modeled wind velocity is correlated with the observed wind velocity obtained from QuikSCAT with a correlation factor of 0.970 (significant level >0.999). The wind intensity is also correctly reproduced: the mean value over LION between December 2004 and March 2005 is equal to 8.32 m s^{-1} in ARPERA versus 9.12 m s^{-1} in QuikSCAT, with a RMSE of 1.67 m s^{-1}.

2.2.2. Lateral Boundary Conditions: River, Black Sea, and Atlantic Forcings

[11] No salinity damping is used at the surface and a freshwater flux due to rivers runoff is explicitly added to

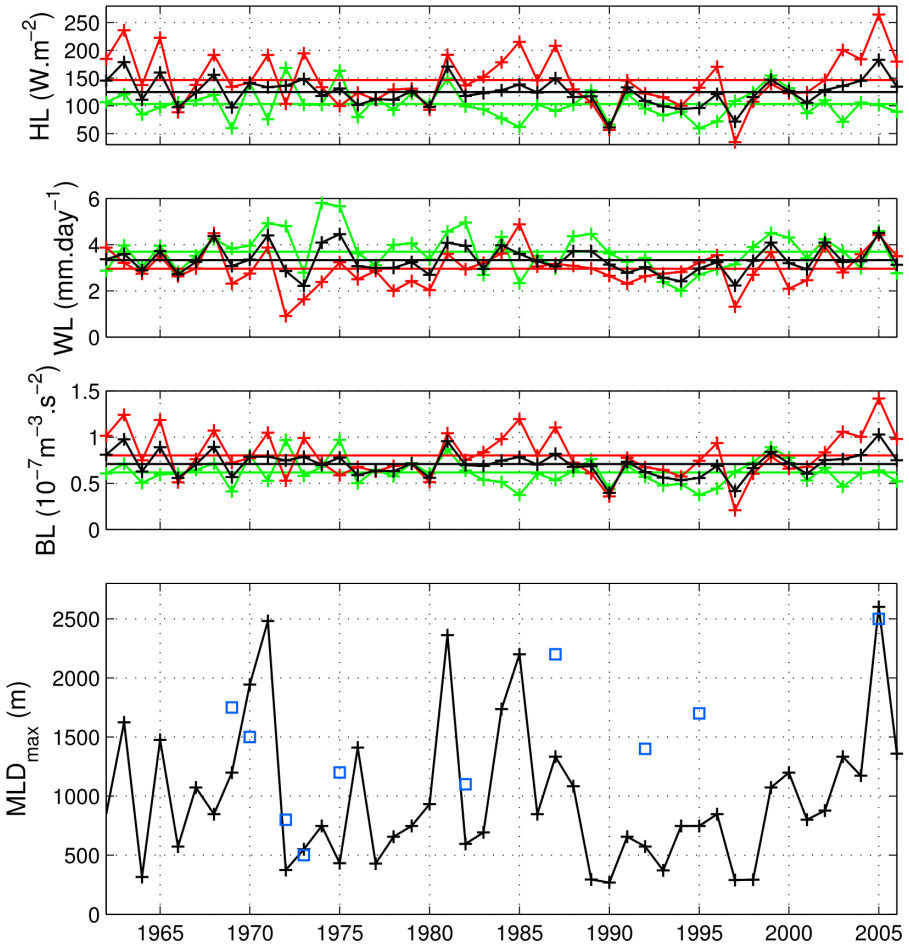

Figure 2. Atmospheric forcing and deep convection: time series of the average autumn (September–November, green), winter (December–February, red), and autumn plus winter (September–February, black) surface heat loss (*HL*), water loss (*WL*), and buoyancy loss (*BL*) over LION in ARPERA and of the winter maximum of the spatial maximum of *MLD* over LION ($MLD_{\max}$) between winter 1961–1962 and winter 2005–2006. Here 1965 corresponds to winter 1964–1965. For the atmospheric fluxes the horizontal lines indicate the mean values over 1961–2005. Blue squares correspond to observed MLD values available through several oceanographic cruises and reported by *Mertens and Schott* [1998], *Testor and Gascard* [2006], and *Schröder et al.* [2006].

complete the surface water budget. Here we use a monthly mean climatology (constant over the years) computed from the RivDis database [*Vörösmarty et al.*, 1996] for the main 33 rivers of the Mediterranean Sea catchment basin.

[12] The Black Sea, not included in NEMOMED8, is one of the major freshwater sources for the Mediterranean Sea. The exchanges between the Black Sea and the Aegean subbasin consist of a two-layer flow across the Marmara Sea and the Dardanelles Strait. We assume that this flow can be approximated by a freshwater flux diluting the salinity of the mouth grid point. Thus, the Black Sea is considered as a river for the Aegean. We use a monthly mean climatology for this net flux based on the data collected by *Stanev et al.* [2000].

[13] The exchanges with the Atlantic Ocean are performed through a buffer zone from 11°W to 7.5°W. Temperature and salinity in this area are relaxed toward the 3-D T-S fields of the seasonal *Reynaud et al.* [1998] climatology by means of a Newtonian damping term in the tracer equation equal to $-(X_{model} - X_{climatology})/\tau$. The restoring term is weak close to the Gibraltar Strait (τ = 100 days at 7.5°W) and stronger moving away from it (τ = 3 days at 11°W).

Figure 3. (a) Time series during winter 2004–2005 of the average over LION of the daily wind velocity in ARPERA (black) and QuikSCAT (gray) and of the surface heat, water, and buoyancy losses (*HL*, *WL*, *BL*) in ARPERA. For the buoyancy loss, the thin black (gray) line corresponds to the contribution of the water loss (BL_W) (heat loss (BL_H)), and the thick line corresponds to the total *BL* (= $BL_H + BL_W$). (b) Time series of the maximum MLD over LION, $MLD_{\max}$, and of the volume of WMDW formed during winter 2004–2005, V_{DW}, for each simulation performed under the atmospheric forcing of 2004–2005 (CI*XX* and year 2004–2005 of CTRL and NEMT).

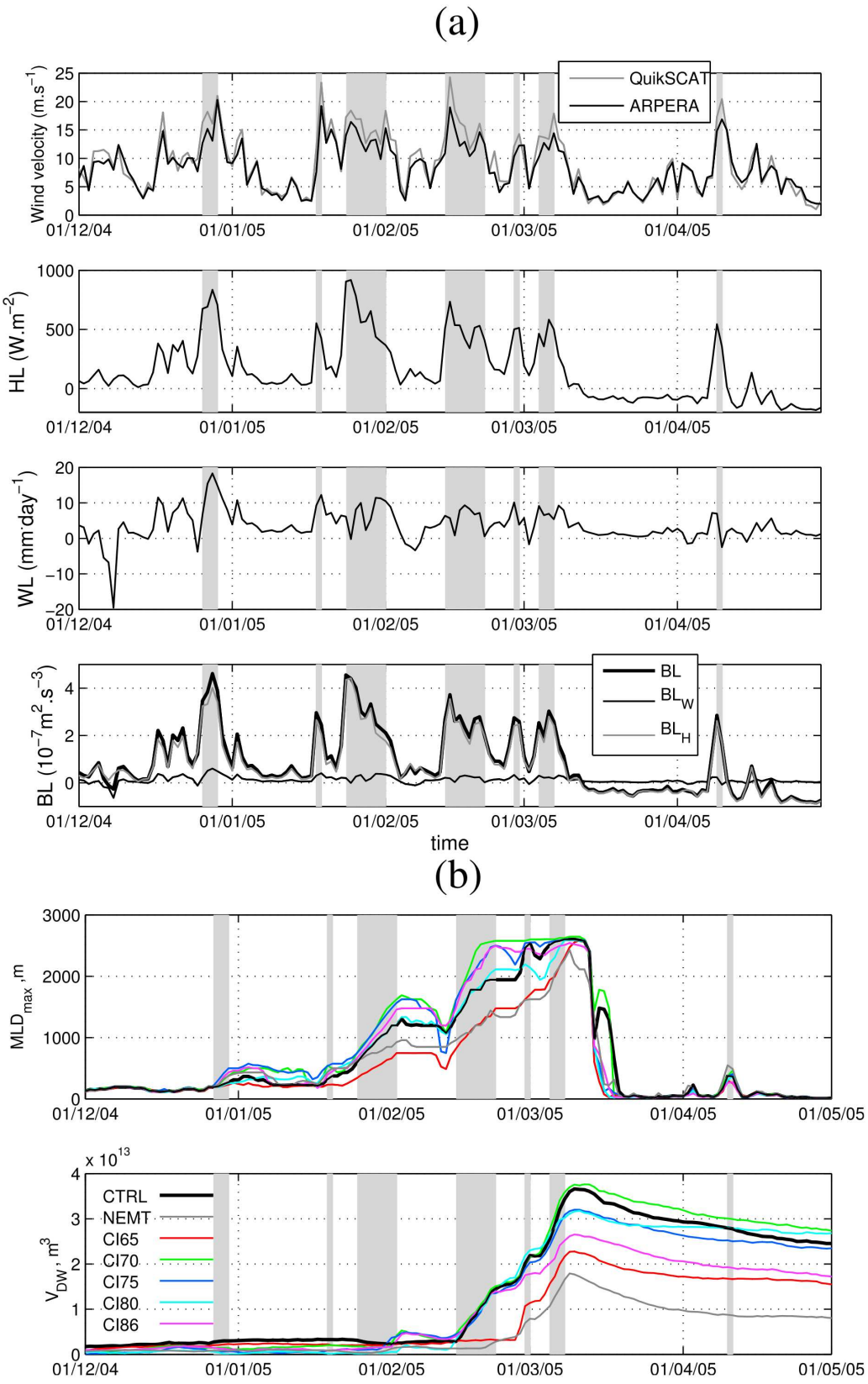
(a)
Wind velocity (m.s^{-1})
QuikSCAT
ARPERA
HL (W.m^{-2})
WL (mm.day^{-1})
BL (10^{-7}m^2.s^{-3})
BL
BL$_W$
BL$_H$
01/12/04
01/01/05
01/02/05
01/03/05
01/04/05
time
(b)
MLD$_{max}$,m
x 10^{13}
V$_{DW}$, m^3
CTRL
NEMT
CI65
CI70
CI75
CI80
CI86
01/05/05

Figure 3

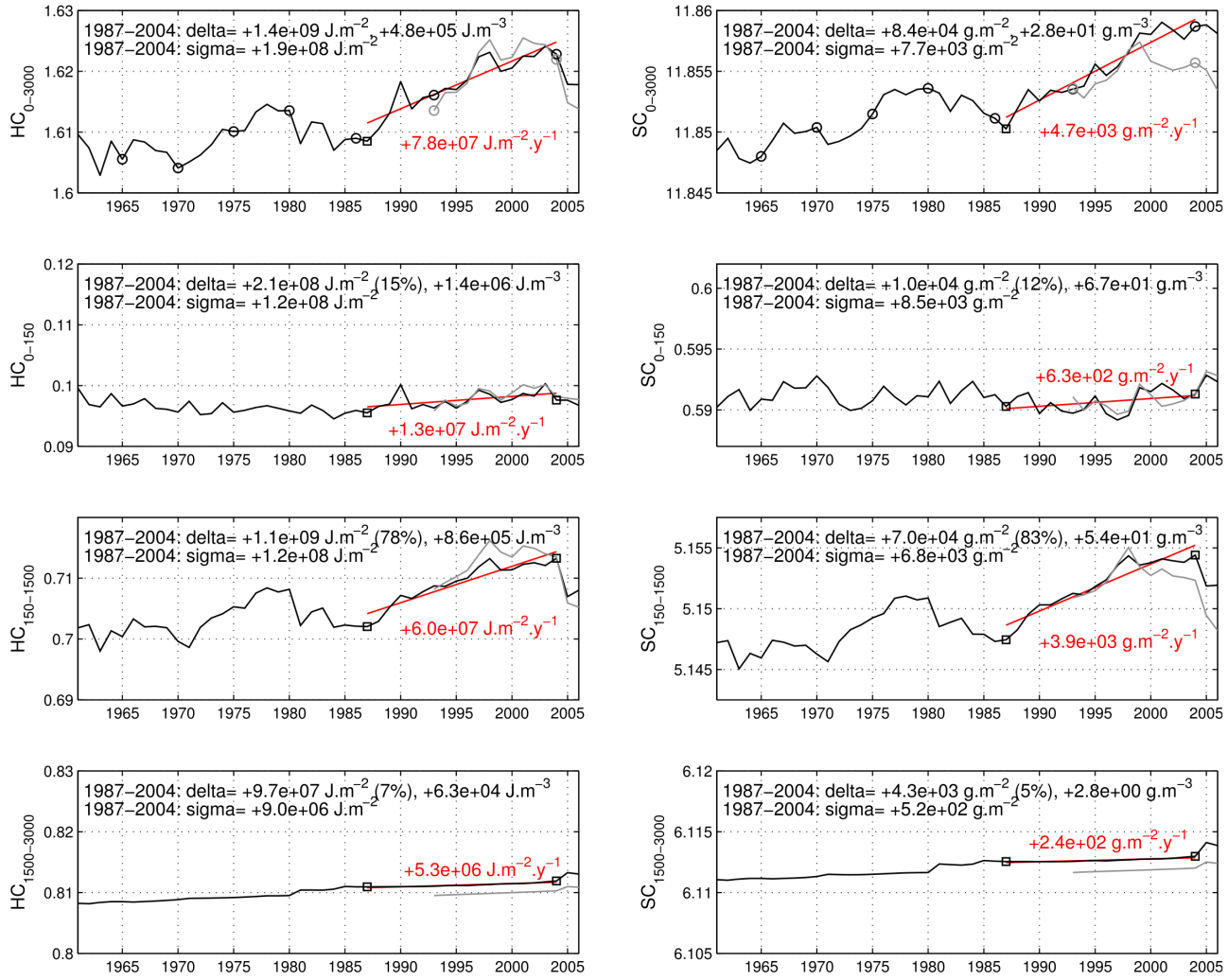

Figure 4. Time series of the mean August (left) heat (*HC*, 10^{11} J m^{-2}) and (right) salt (*SC*, 10^{7} g m^{-2}) contents of the average water column over LION between 1961 and 2006 in CTRL (black) and between 1993 and 2006 in NEMT (gray) for the whole water column (top line) and the layers 0–150 m (second line), 150–1500 m (third line), and 1500 m to bottom (bottom line). The red line shows the trend between 1987 and 2004 in CTRL, obtained from a linear regression analysis. The value of the trend is indicated in red. Delta indicates the variation of those contents between August 1987 and August 2004 in CTRL, the contribution of each sublayer to the total variation, and the variation of the volumic contents. Sigma is the standard deviation of the time series between 1987 and 2004 in CTRL after the trend has been removed. Circles indicate the years selected to perform the sensitivity simulation CI*XX*. Squares indicate years 1987 and 2004.

2.3. Simulations

[14] To answer the scientific questions posed in section 1, we performed several numerical simulations.

2.3.1. Control Simulation CTRL

[15] *Beuvier et al.* [2010] performed an oceanic simulation of the Mediterranean circulation for the 1960–2000 period with NEMOMED8, using the forcings presented above for the surface and lateral boundary conditions (run NM8-ctrl in their paper). The details of this simulation (initial conditions, spin-up) are given in their paper. The initial conditions are given by the MEDATLAS-II climatology [*MEDAR/MEDATLAS Group*, 2002] for the Mediterranean part of the model, and by the *Reynaud et al.* [1998] climatology for the Atlantic buffer zone. A 15 year spin-up was then performed before to launch the simulation in August 1960. *Beuvier et al.* [2010] showed that the EMT was realistically reproduced in this simulation: due to an accumulation of dense water in the Aegean during the 1980s and beginning of the 1990s, plus a strong buoyancy loss over the Aegean during winters 1991–1992 and 1992–1993, very dense water (ρ >29.2 kg m^{-3}) filled 75% of the Aegean in 1993. This water then cascaded through the Cretan Arc sills into the Ionian and Levantine subbasins and propagated through the rest of the Eastern basin. They also validated the evolution over the period 1960–2000 of the heat and salt contents of the different layers of the Mediterranean Sea, by comparing them to the interannual values given by *Rixen et al.* [2005].

Table 2. Simulations Used in This Study[a]

Name	Atmospheric Forcing: ARPERA	Initial Oceanic Conditions
CTRL	Aug 1960 to Aug 2005	After the initial spin-up: Aug 1960
CI65	Aug 2004 to Aug 2005	Aug 1965 of CTRL
CI70	Aug 2004 to Aug 2005	Aug 1970 of CTRL
CI75	Aug 2004 to Aug 2005	Aug 1975 of CTRL
CI80	Aug 2004 to Aug 2005	Aug 1980 of CTRL
CI86	Aug 2004 to Aug 2005	Aug 1986 of CTRL
AF65	Aug 1965 to Aug 1966	Aug 2004 of CTRL
AF70	Aug 1970 to Aug 1971	Aug 2004 of CTRL
AF75	Aug 1975 to Aug 1976	Aug 2004 of CTRL
AF80	Aug 1980 to Aug 1981	Aug 2004 of CTRL
AF86	Aug 1986 to Aug 1987	Aug 2004 of CTRL
NEMT	Aug 1993 to Aug 2005	Aug 1980 of CTRL

[a]Given are name of the simulation, atmospheric forcing used during the simulation, and oceanic conditions at the beginning of the simulation.

[16] For this study, we extended this simulation until 2006, still using the same forcings (ARPERA for the atmospheric fluxes, *Vörösmarty et al.* [1996] for the rivers, *Stanev et al.* [2000] for the Black Sea and *Reynaud et al.* [1998] for the Atlantic Ocean). In the following, this simulation is named CTRL.

2.3.2. Sensitivity Simulations

2.3.2.1. Impact of the Oceanic Conditions on the Deep Convection Event: Simulations CI*XX*

[17] To investigate the influence of oceanic conditions on the convection event, we performed a first group of sensitivity simulations varying the oceanic conditions before the beginning of the convection event, i.e., in August 2004. For that, we selected contrasted initial oceanic conditions from the CTRL simulation: we considered the mean August heat and salt contents over the whole water column in LION (Figure 4) and selected five contrasted oceanic conditions before the beginning of the EMT, i.e., before 1987: 1965, 1970, 1975, 1980 and 1986. The heat and salt contents over LION, *HC* (unit: J m^{-2}) and *SC* (unit: g m^{-2}), are computed using the following formula:

$$HC = \frac{1}{A_{LION}} \times \iiint_{LION} c_p \rho(x,y,z) T(x,y,z) dxdydz$$
$$SC = \frac{1}{A_{LION}} \times \iiint_{LION} \rho(x,y,z) S(x,y,z) dxdydz \quad (2)$$

where $A_{LION} = 9.40\ 10^{10}$ m^2 is the surface of the LION area. The division by A_{LION} is done in order to obtain an average surfacic value for a column of 1 m^2 of the LION area, so that we will be able to compare it with the surface and lateral fluxes in the following. Five simulations were then launched in August 2004 using those oceanic conditions as initial conditions, and the same atmospheric conditions as CTRL, i.e., ARPERA from August 2004. Those simulations are named CI65, CI70, CI75, CI80 and CI86 in the following.

2.3.2.2. Impact of the Atmospheric Conditions on the Deep Convection Event: Simulations AF*XX*

[18] We performed a second group of sensitivity simulations in order to investigate the influence of atmospheric forcing during the convection event: we ran five simulations from August to May taking the same initial oceanic conditions, those of August 2004 of CTRL, but varying the atmospheric forcing. For that we took the atmospheric forcing of August 1965 to May 1966, August 1970 to May 1971, August 1975 to May 1976, August 1980 to May 1981 and August 1986 to May 1987 from ARPERA. Those simulations are named AF65, AF70, AF75, AF80 and AF86 in the following.

2.3.2.3. Impact of the EMT on the 2005 Convection Event: Simulation NEMT

[19] One of our main objectives is to determine the impact of the EMT on the NWMED convection event of 2004–2005. For that, we performed an additional simulation beginning in August 1993, i.e., just after the EMT, but with the oceanic conditions of August 1980, which are close to August 1993 from the point of view of the heat and salt contents (see Figure 4). This simulation is called NEMT. It cannot contain the EMT signal that occurred between 1987 and 1993, but it is influenced by the same long-term (1993–2004) external forcings as CTRL (surface, hydrologic and lateral boundary conditions). The differences between NEMT and CTRL can therefore be mainly attributed to the impact of the EMT.

[20] The characteristics of the simulations performed for this study are summarized in the first three columns of Table 2: name of the simulation, atmospheric forcing and initial oceanic conditions.

3. Results

3.1. Characteristics of the NWMED Water Column Between 1960 and 2004: Long-Term Evolution and Influence of the EMT

[21] In this section we examine the factors responsible for the evolution until autumn 2004 of the oceanic conditions in the NWMED in terms of heat and salt contents and structure of the water column.

3.1.1. Evolution of the Heat and Salt Contents

[22] *Schroeder et al.* [2010] observed that the salt and heat contents of the water column in the NWMED were anomalously high in 2004. This is reproduced in the CTRL simulation: between August 1987 and August 1998, the heat and salt contents in LION increase regularly, then remain relatively stable until August 2004 (Figure 4). As a result, between 2000 and 2004, these contents are the highest of the whole 1960–2005 period. Between 1987 and 2004, the variation of heat and salt contents are equal to 1.4 10^9 J m^{-2} and 8.4 10^4 g m^{-2}, respectively. Performing a linear regression analysis, we compute trends of those contents between 1987 and 2004 of + 7.8 10^7 J m^{-2} yr^{-1} and + 4.7 10^3 g m^{-2} yr^{-1}, respectively. The standard deviations of the detrended signals are equal to 1.9 10^8 J m^{-2} and 7.7 10^3 g m^{-2}, respectively: those values are 1 order smaller than the values of the variation between 1987 and 2004. The increase observed during this period is therefore statistically significant and not simply due to the interannual variability.

[23] *Schroeder et al.* [2008] suggested that these anomalously high contents could be partly due to an anomalously high arrival of heat and salt from the Eastern basin. However, the regularity of this increase in the model suggests that it is not the case. Moreover, the evolution of the heat and salt contents is very similar in NEMT (Figure 4), which, by construction, does not contain any signal due to the EMT contrary to CTRL. This shows that this increase of heat and salt contents, whatever its origin, was not related to the

EMT. Note that on 1 December 2004, the heat contents are quasi equal in NEMT and CTRL, but that the salt content is slightly higher in CTRL. This suggests that the EMT accentuated the salt content increase, perhaps by increasing the salt content of the intermediate and deep water masses originating from the Eastern basin and circulating in the NWMED. Nevertheless this effect is small compared to the long-term increase occurring during the 1990s.

[24] *Schroeder et al.* [2010] observed that the high heat and salt contents in 2004 were related to an intermediate layer warmer and saltier than the average: they showed that the difference compared to the climatology was the strongest in the 500–1000 m layer. The evolution of the heat and salt contents in each main layer of the average water column over LION in CTRL and NEMT is indicated in Figure 4: surface layer of Atlantic Water (0–150 m), intermediate layer of Levantine Intermediate Water (LIW, 150–1450 m) and deep layer of WMDW (1450 m to bottom). The values obtained for the variation of heat and salt contents between 1987 and 2004 in each layer are indicated for CTRL in Figure 4, as well as the values of the contribution of each layer to the total variation, the trend between 1987 and 2004, and the standard deviation of the detrended signal between 1987 and 2004. In the intermediate and deep layers, the 1987–2004 variation is 1 order of magnitude larger than the standard deviation of the detrended signal. The increase in these layers is therefore significant and not due to the interannual variability. On the contrary, in the surface layer, the variation between 1987 and 2004 is of the same order than the standard deviation of the detrended signal: the difference between 1987 and 2004 cannot be clearly attributed to a positive trend, but is rather due to the interannual variability. This can be explained by the fact that contrary to the deep and intermediate layers, the surface layer is directly submitted to the strong seasonal variability of the atmospheric forcing. Finally during the 1990s, the heat and salt contents significantly increase only in the deep and intermediate layers. The warming and salting of the whole water column is mainly due to the warming and salting of the intermediate layer that represent 78% and 83%, respectively, of the total increase.

[25] The evolution between 1961 and 2006 in CTRL of the yearly maximum of the spatial maximum of the daily mixed layer depth (MLD) over LION, $MLD_{\max}$, is presented in Figure 2 (black line for CTRL). Comparing the evolution of $MLD_{\max}$ with the evolution of the total heat and salt contents shows that those contents increase during the periods of weak convection (1971–1979, 1988–1998) and decrease or remain approximately constant during the periods of stronger convection (1961–1970, 1981–1987, 1999–2006). Indeed, when deep convection occurs, the water column is mixed, producing WMDW. When convection ceases after the winter, the salt and heat originally contained in the warm and salty intermediate layer are exported with the WMDW in the deep layer then out of the convection area [*Herrmann et al.*, 2008]. This results in a transfer of heat and salt from the intermediate layer into the deep layer. This abrupt removal (input) of heat and salt from the intermediate layer (into the deep layer) was observed by *Schroeder et al.* [2010] after the convection event of winter 2004–2005. It is reproduced in CTRL, for example after the strong convection events of winters 1980–1981 and 2004–2005, that both occurred after several winters without deep convection (Figures 4 and 2). Salt and heat are then progressively reintroduced in the intermediate layer when the salty and warm LIW originating from the Eastern basin [*Millot*, 1999] spreads into the NWMED. If convection does not occur during a few years, the heat and salt contents of the intermediate layer will therefore increase until warm and salty LIW has completely refilled this layer. As will be shown in section 3.3.1, the intensity of deep convection depends on the winter buoyancy loss: deep convection occurs when the winter buoyancy loss is sufficiently strong, enabling the initially stratified water column to be mixed to great depth. Between 1988 and 2001, the winter buoyancy loss was generally lower than the average, explaining that convection was weak during this period (Figure 2). Our results therefore suggest that the exceptionally high heat and salt contents in 2004 were not due to an anomalously high arrival of heat and salt induced by the EMT, but to the absence of strong convection during the 1990s. This absence would have resulted from the weakness of the winter atmospheric buoyancy loss during this period and enabled the heat and salt to accumulate in the intermediate layer.

[26] Observed values of MLD available thanks to several oceanographic campaigns reported by *Mertens and Schott* [1998], *Testor and Gascard* [2006] and *Schröder et al.* [2006] are also indicated in Figure 2 (blue squares). Comparing the data and the model results suggests that the absolute value of the modeled MLD is generally underestimated. Data are, however, too scarce to validate the representation of the interannual variability of the MLD, which is suggested here to play an important role in the long-term evolution of heat and salt content in the Gulf of Lion. Nevertheless, this comparison put our conclusions into perspectives, reminding that they are obtained thanks to a given model forced by a given atmospheric data set. We analyze and interpret the results of this model, which is not the reality but a tentative to represent it as well as possible using the state of the art of the models used to simulate the long-term Mediterranean oceanic circulation. It would be necessary to perform a group of other simulations using other ocean models and other atmospheric forcing in order enforce the robustness of our conclusions or to propose alternative explanations. Note, however, that other studies [*Sannino et al.*, 2009] also suggest that due to weak winter surface buoyancy flux, the 1990s was a period of weak convection.

3.1.2. Impact of the EMT on the Structure of the Water Column

[27] Analyzing hydrographic data, *Gasparini et al.* [2005] showed that in the Sicily channel and in the Tyrrhenian subbasin, the EMT resulted in a deepening between 1992 and 2003 of the heat and salt originating from the Eastern Basin. As a result the saltier and warmer waters progressively extended their influence in depth until 1500 m (see Figure 14 of *Gasparini et al.* [2005]). Deep water of eastern origin then flows into the NWMED [*Millot*, 1999], we can therefore expect from those observations in the Tyrrhenian that the EMT induced the deepening of the salty and warm intermediate layer in the NWMED. Indeed, the heat and salt increase extended deeper in CTRL (until 1500 m; Figure 5), in agreement with the observations, than in NEMT where it mainly occurred in the "classical" intermediate layer (200–1000 m). Our modeling study therefore shows an effect of

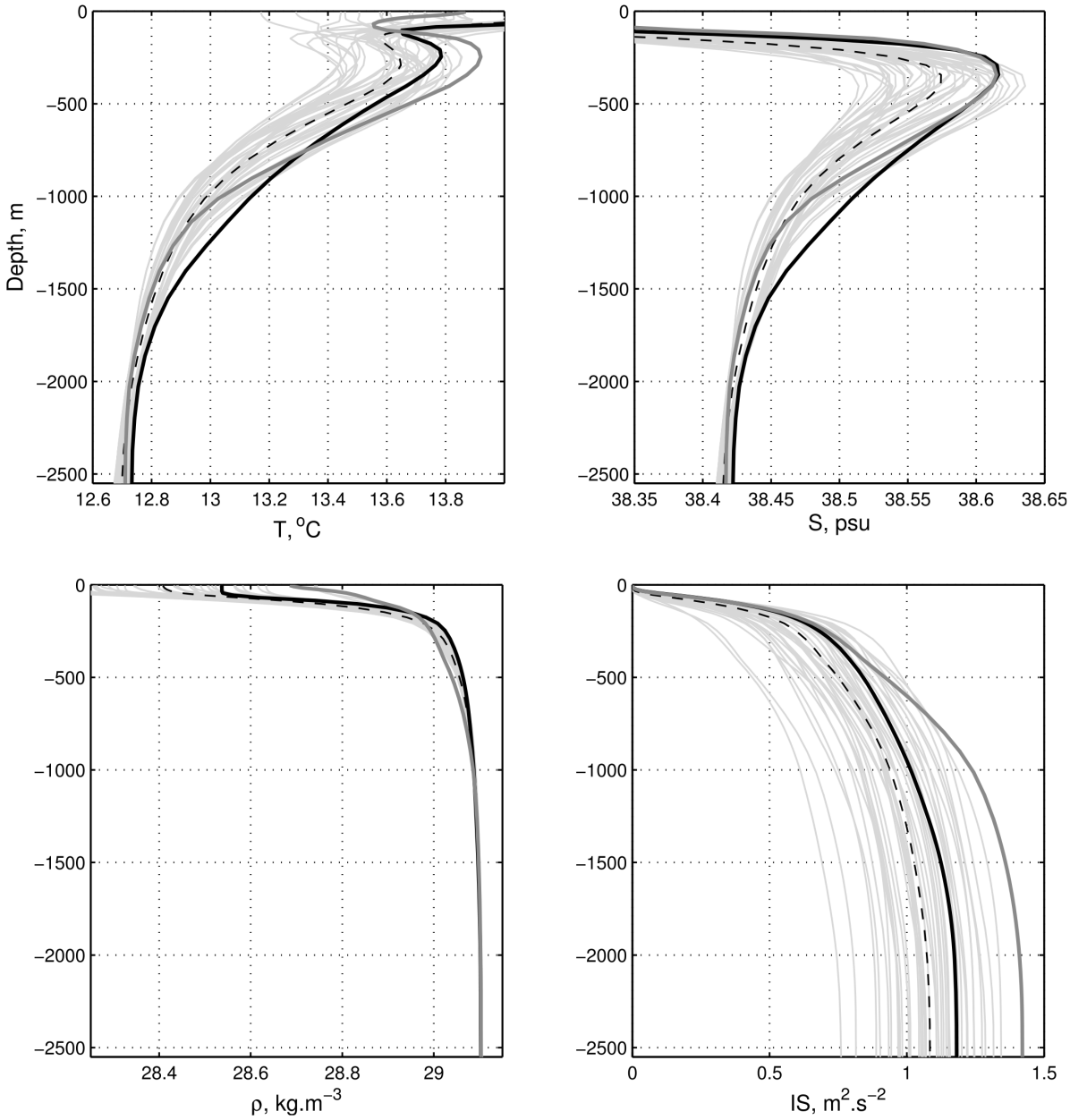

Figure 5. Average temperature, salinity, density, and stratification profiles in December over LION. Light gray lines are 1961–2000 for CTRL. Dashed line is average profile over 1961–2000. Black line is 2004 for CTRL. Dark gray line is 2004 for NEMT.

the EMT on the structure of the NWMED water column in agreement with the observations made by *Gasparini et al.* [2005] and *Schroeder et al.* [2010]: the EMT induced a deepening of the heat and salt maximum in the NWMED.

[28] *Gasparini et al.* [2005] showed that this deepening was associated with an increase of the density of the warm and salty eastern waters flowing in the intermediate and deep layers of the Western basin. This increase of the density in the intermediate layer is reproduced by the model, as can be seen when comparing the CTRL and NEMT density profiles (Figure 5). The vertical density gradient in these layers consequently decreased. To investigate the effect of this modification of the density profile on the stratification of the NWMED water column, we compute the total buoyancy flux required to mix an initially stratified water column down to the depth z, $IS(z)$, using the formula used by *Herrmann et al.* [2008]:

$$IS(z) = \int_0^z N^2(h).h.dh = \int_0^z \frac{-g}{\rho}\frac{\partial \rho}{\partial h}.h.dh \qquad (3)$$

where N (s^{-1}) is the initial Brunt-Väisälä frequency. IS represents an index of the stratification of the water column. The stratification profiles on December 2004 over LION are shown in Figure 5 for CTRL and NEMT. The stratification in NEMT is among the strongest of the whole 1961–2004 period, whereas the stratification in CTRL is only slightly above the average. This shows that the EMT induced a

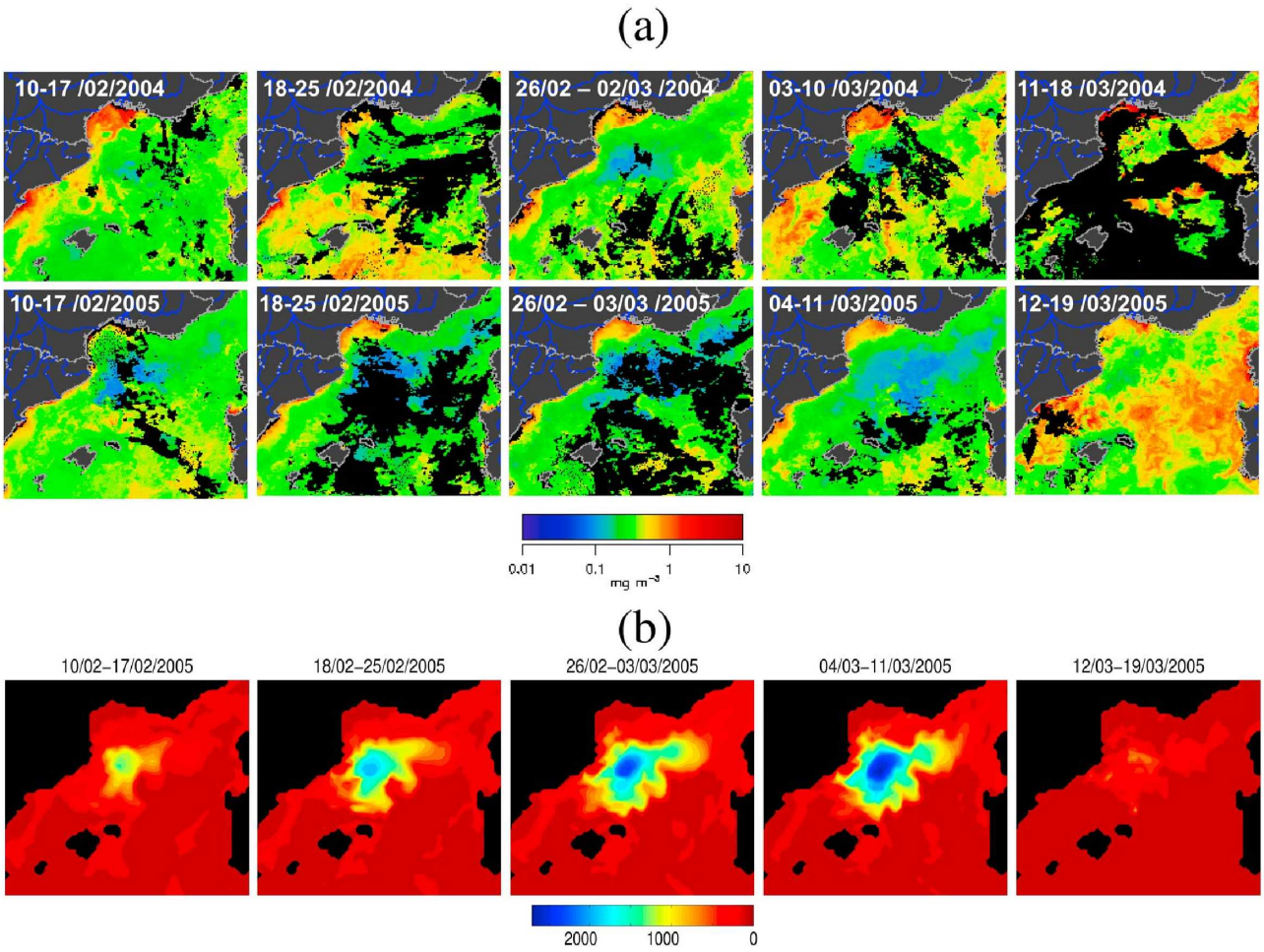

Figure 6. (a) Weekly averaged surface chlorophyll concentration observed by MODIS in the NWMED during the winter convection period (mid-February/mid-March) in (top) 2004 and (bottom) 2005 (unit is mg m^{-3}). (b) Maps of the MLD averaged over the same periods in CTRL (unit is meters).

weakening of the NWMED stratification compared with what would have been the case without the EMT. This is due to the fact that $IS(z)$ being proportional to $\int z \times \frac{\partial \rho}{\partial z}$, a decrease of the vertical density gradient in the intermediate and deep layer results in a decrease of IS.

3.2. Modeling of the 2005 NWMED Convection Event: Validation of the CTRL Simulation

[29] All the information concerning the 2004–2005 convection event available to us was gathered in order to validate the modeling of this event in CTRL. First, in situ observations available in the literature cited in section 1 provide information about the hydrologic characteristics and the structure of the water column in the WMED and about the characteristics of the WMDW. Second, satellite ocean color data provide information about the temporal and spatial evolution of the convection process.

3.2.1. Temporal and Spatial Characteristics of the 2005 Convection Event

[30] The deepest value of MLD_{max} between 1961 and 2006 in CTRL is obtained for 2004–2005 (2601 m), one of the four winters of the whole period during which the convection reaches the bottom (MLD >2000 m) in this simulation (Figure 2). Convection during winter 2004–2005 is therefore exceptionally strong in CTRL, in agreement with the reported observations.

[31] MODIS Ocean color data available on http://marine.jrc.ec.europa.eu provide an estimate of the extension of the convection area. In this area, strong vertical displacements indeed prevent the phytoplankton from remaining at the surface. The convection area therefore corresponds to the region of low chlorophyll concentration. Figure 6a shows the maps of the 8 day average chlorophyll obtained from MODIS between 10 February and 18 March 2004 and 2005. Comparing the 2004 and 2005 maps shows that the particularly large extension of the convection area in 2005 is well captured by those images.

[32] The extension of the low chlorophyll area is the largest between 18 February and 11 March 2005, indicating that this period was the period of maximum convection. Convection does not seem to occur after 12 March. This is in agreement with *Smith et al.* [2008] who reported that the water column was strongly mixed in the Catalan sea between 7 and 12 March.

[33] WMDW is identified in our simulations as the water of density larger than 29.1 kg m^{-3}, following previous

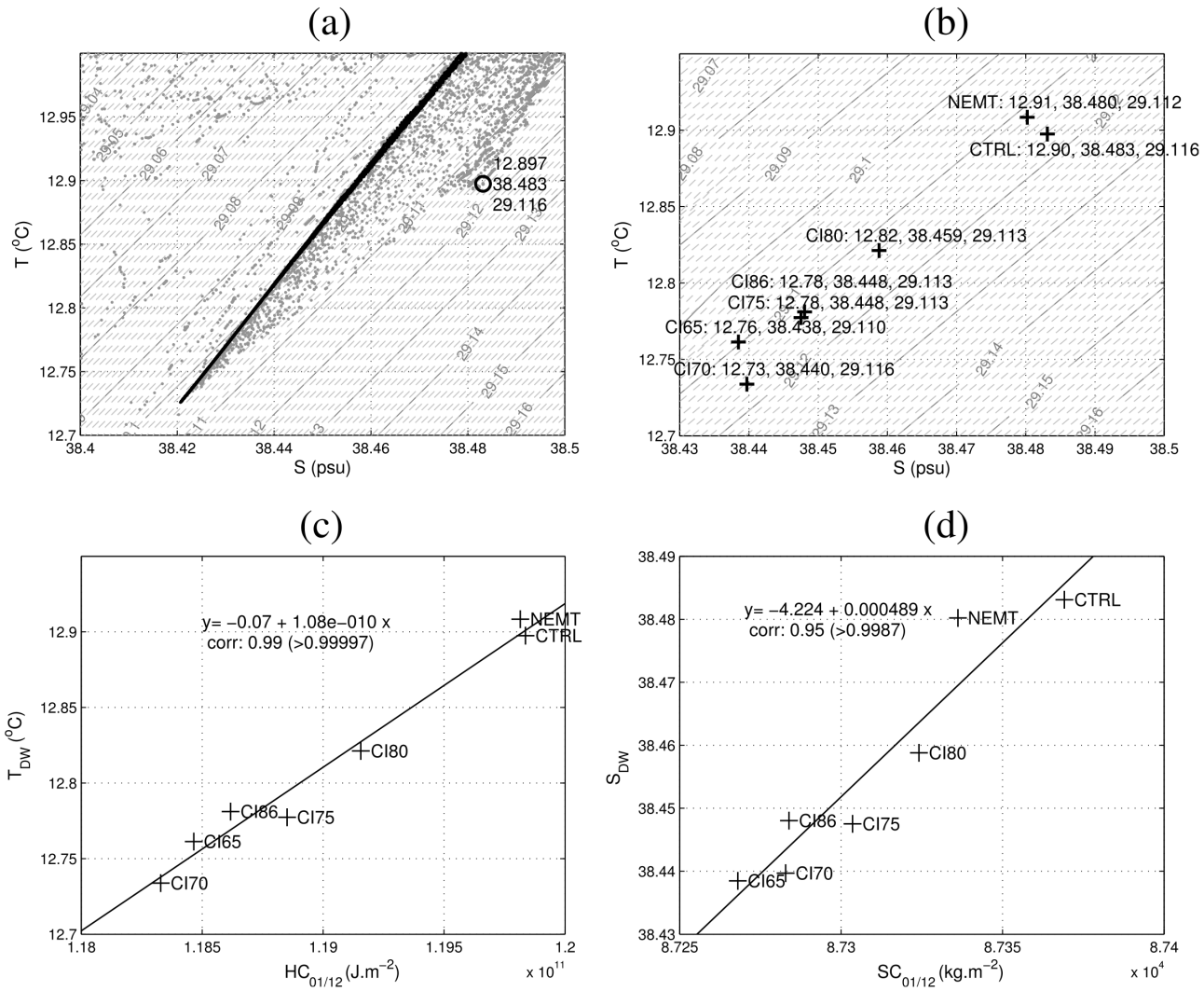

Figure 7. WMDW characteristics in simulations performed under the atmospheric forcing of 2004–2005. (a) Temperature-salinity diagram of the water present in LION over the whole column before the convection (1 December 2004, black points) and at the date of maximum convection (10 March 2005, gray points) in CTRL: each point corresponds to a point of the model grid. The characteristics of the densest water present in LION on 10 March 2005 are indicated (black circle). (b) Characteristics (T (°C), S, ρ (kg m^{-3})) of the densest water present in LION at the date of maximum convection (10 March 2005) for each simulation. (c) Relation between the preconvection heat content over LION, $HC_{01/12}$, and the WMDW temperature T_{DW}. (d) Relation between the preconvection salt content over LION, $SC_{01/12}$, and the WMDW salinity S_{DW}.

modeling and observation studies [see, e.g., *Marshall and Schott*, 1999; *Herrmann et al.*, 2008]. Following *Herrmann et al.* [2008], the volume of newly formed WMDW V_{DW} is computed each day as the difference between the volume of WMDW present in the NWMED on this day and the minimum of this volume before the convection event, i.e., in autumn 2004 (equal to 13.0 10^{13} m^3): V_{DW} represents an anomaly. The WMDW formation rate τ_{DW} is then computed following *Castellari et al.* [2000] by dividing V_{DW} by the numbers of seconds in 1 year. Times series between 1 December 2004 and 30 April 2005 of the modeled maximum MLD over LION $MLD_{\max}$ and of V_{DW} are shown in Figure 3b (black line for CTRL). The evolution of the convection event follows the atmospheric chronology: each atmospheric event of strong buoyancy loss induces an abrupt increase of $MLD_{\max}$ and V_{DW}. The mixed layer reaches 1500 m on 17 February, and the bottom is reached between 27 February and 13 March ($MLD_{\max}$ > 2000 m), with a small decrease between 1 March and 3 March induced by a decrease of buoyancy loss. This is in agreement with the satellite and in situ observations. The maximum of V_{DW} is reached on 10 March after the last atmospheric event. It is equal to 3.66 10^{13} m^3, corresponding to a formation rate τ_{DW} of 1.16 Sv. This value is consistent with *Schroeder et al.* [2008], who estimated from in situ observations that the cumulated formation rate for winters 2004–2005 and 2005–2006 was approximately equal to 2.4 Sv. Then, as soon as the atmospheric BL becomes negative, $MLD_{\max}$ abruptly decreases to zero: restratification of the water column begins, and V_{DW} starts to decrease. The chronology of

Table 3. Preconvection and Convection Characteristics for Each Simulation[a]

Name[b]	HC on 1 December (10^{11} J m^{-2})	SC on 1 December (10^4 kg m^{-2})	IS on 1 December (m^2 s^{-2})	T_{DW} (°C)	S_{DW}	ρ_{DW} (kg m^{-3})	τ_{DW} (Sv)	$MLD_{\max}$ (m)	MLD_{mean} (m)
CTRL 2004–2005	1.198	8.737	1.02	12.90	38.483	29.116	1.16	2601	943
CTRL 1965–1966	1.184	8.727	1.11	no WMDW			0.07	372	94
CTRL 1970–1971	1.185	8.729	1.02	12.81	38.451	29.110	0.42	2398	472
CTRL 1975–1976	1.186	8.731	0.90	no WMDW			0.14	1416	264
CTRL 1980–1981	1.188	8.733	0.84	12.90	38.479	29.113	0.85	2382	510
CTRL 1986–1987	1.188	8.728	1.21	no WMDW			0.06	1333	223
CI65	1.185	8.727	1.15	12.76	38.438	29.110	0.72	2584	729
CI70	1.183	8.728	0.98	12.73	38.440	29.116	1.19	2645	923
CI75	1.189	8.730	1.05	12.78	38.448	29.113	1.02	2604	804
CI80	1.192	8.732	1.05	12.82	38.459	29.113	1.01	2593	749
CI86	1.186	8.728	1.10	12.78	38.448	29.113	0.84	2543	765
AF65	1.198	8.737	1.01	no WMDW			0.06	433	118
AF70	1.200	8.737	1.06	13.04	38.513	29.110	0.54	1883	564
AF75	1.196	8.737	0.86	no WMDW			0.10	1199	282
AF80	1.195	8.738	0.77	12.92	38.488	29.115	1.63	2562	768
AF86	1.200	8.736	1.15	no WMDW			0.08	1333	291
NEMT 2004–2005	1.198	8.734	1.24	12.91	38.480	29.112	0.57	2429	746

[a]Given are average heat and salt contents and stratification index at 1000 m over LION on 1 December (HC, SC, and IS), WMDW characteristics (T_{DW}, S_{DW}, and ρ_{DW}), WMDW formation rate (τ_{DW}), winter maximum of the maximum MLD over LION ($MLD_{\max}$), and winter maximum of the average MLD over LION (MLD_{mean}). When $MLD_{\max} < 1500$ m the convection is not considered as deep but intermediate. No WMDW is formed.
[b]Year is also given for CTRL and NEMT.

the convection event reproduced by the model is therefore in good agreement with the chronology deduced from the available observations.

[34] The modeled area of convection corresponds to the area obtained from the ocean color data, as can be seen when comparing the maps of the 8 day average of the modeled MLD between 10 February and 18 March shown in Figure 6b and the corresponding ocean color maps. At each period, the size and position of the modeled convection area corresponds to the size and position of the observed low chlorophyll concentration area. The extension of the convection area is the largest between 26 February and 11 March, as the extension of the low chlorophyll concentration area.

3.2.2. Characteristics of WMDW Formed in 2005

[35] Figure 7a shows the temperature-salinity diagram of the water present in LION before the convection event (1 December 2004) and when the convection reaches its maximum (10 March 2005). "Old" WMDW, i.e., WMDW formed before winter 2004–2005, can be identified on 1 December as the water present in LION and denser than 29.10 kg m^{-3}: in CTRL, characteristics of old WMDW are ~12.72–12.80°C and ~34.42–38.44. They belong to the range of the observed characteristics of old WMDW reported in the literature (12.75–92°C, 38.41–47; see Table 1). WMDW formed during winter 2004–2005 can be identified as the densest water present on 10 March. Its characteristics (T_{DW} = 12.90°C, S_{DW} = 38.48 and ρ_{DW} = 29.116 kg m^{-3}) are in very good agreement with the observed characteristics of WMDW formed in 2005 (12.87–90°C, 38.47–50, 29.113–130 kg m^{-3}; see Table 1). The change of temperature and salinity between old and "new" WMDW is therefore also correctly reproduced (~+0.1–0.2°C and ~+0.04–0.06).

3.3. Analysis of the Sensitivity Simulations: Which Factors Were Responsible for the Characteristics of the 2005 Convection Event?

[36] Having shown that the CTRL simulation represents correctly the 2004–2005 convection event, we now analyze the sensitivity simulations in order to determine the respective contributions of the oceanic and atmospheric conditions to the characteristics of this event.

3.3.1. Why Was the 2004–2005 Convection Event Exceptionally Strong?

[37] In this section we investigate the factors responsible for the exceptional intensity of the 2005 convection event in terms of mixed layer depth and volume of newly formed WMDW: we examine the influence of the stratification of the water column at the beginning of the convection, of the EMT and of the atmospheric conditions during 2004.

3.3.1.1. Impact of the Oceanic Conditions of 2004–2005 and of the EMT on the Convection Intensity

[38] To investigate the role played by the oceanic conditions in the intensity of the 2004–2005 convection event, we examine the simulations where the atmospheric forcing is the one of year 2004–2005 but where the initial oceanic conditions vary: CI*XX* and year 2004–2005 of CTRL and NEMT. For those simulations, the evolution of the maximum MLD over LION, $MLD_{\max}$, and of the volume of newly formed WMDW, V_{DW}, is presented in Figure 3b. The chronology of the convection event is the same for all those simulations: each event of strong atmospheric buoyancy loss (highlighted in gray in Figure 3) induces an abrupt deepening of the mixed layer and an increase of V_{DW}, which then remain relatively stable. The maximum of the convection intensity, corresponding to the maximum of V_{DW}, is reached for all the simulations on 10 March, just after the last event of strong buoyancy loss occurring in March. At this time, the convection reaches the bottom in all the simulations: $MLD_{\max}$ varies between 2430 m for NEMT and 2645 m for CTRL (Table 3). The MLD then abruptly decreases when the buoyancy loss becomes positive, after 13 March, and V_{DW} begins to decrease.

[39] First, this shows that the chronology of the convection in terms of deepening/shallowing of the mixed layer and increase/decrease of V_{DW} is driven by the succession of atmospheric events. For year 2004–2005, this resulted in a strong bottom convection. Second, although bottom convection occurs in all those simulations, the volume of newly

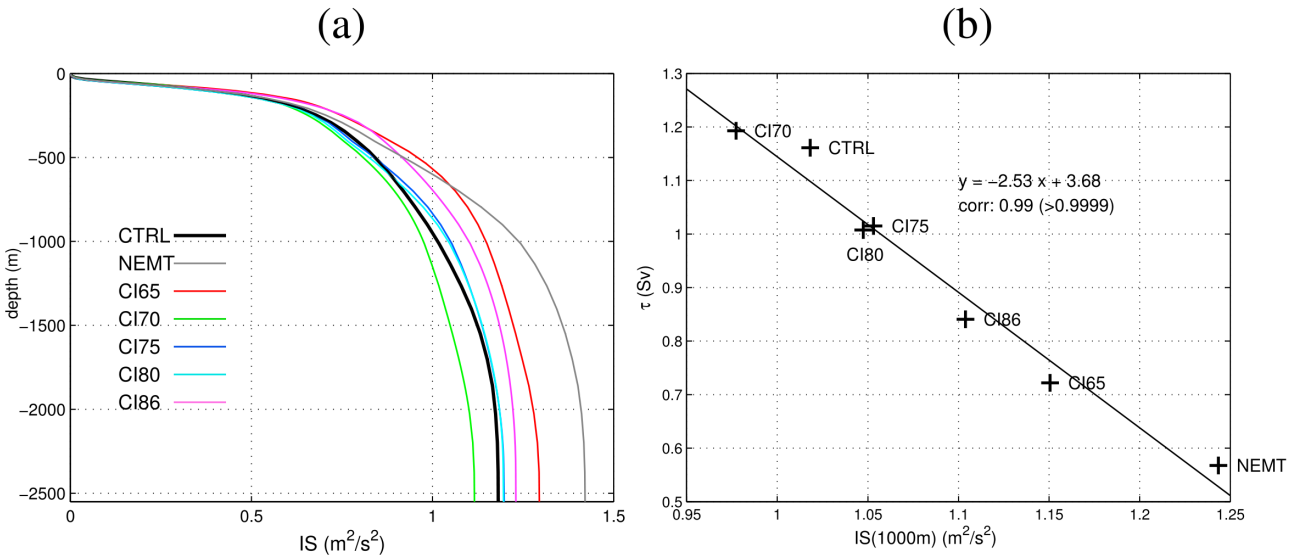

Figure 8. (a) For simulations performed under the 2004–2005 atmospheric forcing, average profile over LION of the stratification index on 1 December, $IS(z)$. (b) Relation between the average stratification index over LION at 1000 m on 1 December 2004, $IS(1000m)$, and the WMDW formation rate, τ_{DW}.

formed WMDW varies by a factor of 2 between the most and the less productive simulations ($\tau_{DW} \sim 0.7$ Sv in CI65 and ~1.2 Sv in CI70; Figure 3b and Table 2). This variability of τ_{DW} is actually related to the variability of the stratification of the water column at the beginning of the convection: the more stratified the column is, the more difficult it is to mix it. To show that, we examine the profiles of $IS(z)$ before the convection event on 1 December for year 2004 of NEMT, CTRL and CI*XX* (Figure 8a). The most stratified water column is obtained in NEMT, and CTRL is among the simulations with the less stratified water column. The largest winter maximum of the average *MLD* over LION in 2005 is obtained for CTRL: MLD_{mean} = 943 m, slightly less than 1000 m (Table 3). We therefore compute for each simulation the stratification index of the water column at 1000 m before the convection event on 1 December 2004 (Table 2). Performing a regression analysis between the WMDW formation rate τ_{DW} and IS(1000 m, 1 December 2004), we obtain a strong linear relationship with a correlation factor of 0.99 (SL >0.9999) (Figure 8b). For given atmospheric conditions, here those of winter 2004–2005, the variability of the intensity of deep convection in terms of volume of newly formed WMDW is therefore directly related to the variability of the stratification at the beginning of the convection, which facilitates or hinders the mixing of the water column.

[40] Comparing the *IS* profiles in December 2004 in NEMT and CTRL, we showed in section 3.1 that the EMT induced a weakening of the stratification in the NWMED. As a result, the intensity of deep convection in terms of WMDW formed is twice stronger in CTRL than in NEMT.

3.3.1.2. Impact of the Atmospheric Conditions of 2004–2005 on the Convection Intensity

[41] Figure 5 shows the profiles of $IS(z)$ before the convection event on 1 December for all the years of the CTRL simulation and for year 2004 of NEMT. The water column on 1 December 2004 in NEMT is the most stratified of all the years; however, the convection reaches the bottom. This suggests that the atmospheric buoyancy loss in 2004–2005 played the most determining role in the intensity of the convection event: it was so strong that convection could have reached the bottom even for the most stratified conditions.

[42] To confirm the influence of the atmospheric conditions on the intensity of the 2004–2005 convection event, we examine the simulations where the initial oceanic conditions are those of August 2004 but where the atmospheric forcing varies: AF*XX* and year 2004–2005 of CTRL. For those simulations, the evolution of the atmospheric buoyancy loss, of $MLD_{\max}$ and of V_{DW} is presented in Figure 9. The variability of the convection depth and newly formed WMDW volume induced by the atmospheric forcing is much larger than the variability induced by the oceanic conditions: there are simulations with no convection (AF65, $MLD_{\max}$ = 433m) or intermediate convection (1000 m < $MLD_{\max}$ < 1500 m, AF70, AF86) and practically no WMDW formed ($\tau_{DW} < 0.1$ Sv), and simulations with τ_{DW} varying between 0.5 Sv and 1.6 Sv with deeper convection (AF75, $MLD_{\max}$ = 1883m) or even bottom convection ($MLD_{\max}$ > 2000 m, AF80, CTRL). This confirms that the factor predominantly responsible for the intensity of deep convection in 2004–2005 was the atmospheric forcing rather than the oceanic conditions: with different initial oceanic conditions of another autumn bottom convection would have occurred anyway, whereas with different atmospheric conditions there could have been no convection, intermediate convection or bottom convection.

[43] Which aspect of the atmospheric forcing more precisely drives the convection? We saw that the succession of strong buoyancy loss event induces the deepening of the mixed layer during the winter, corresponding to the violent mixing phase of deep convection defined by *Marshall and Schott* [1999]. We therefore expect the variability of the intensity of deep convection to be related to the variability of the cumulated buoyancy loss over this phase. However,

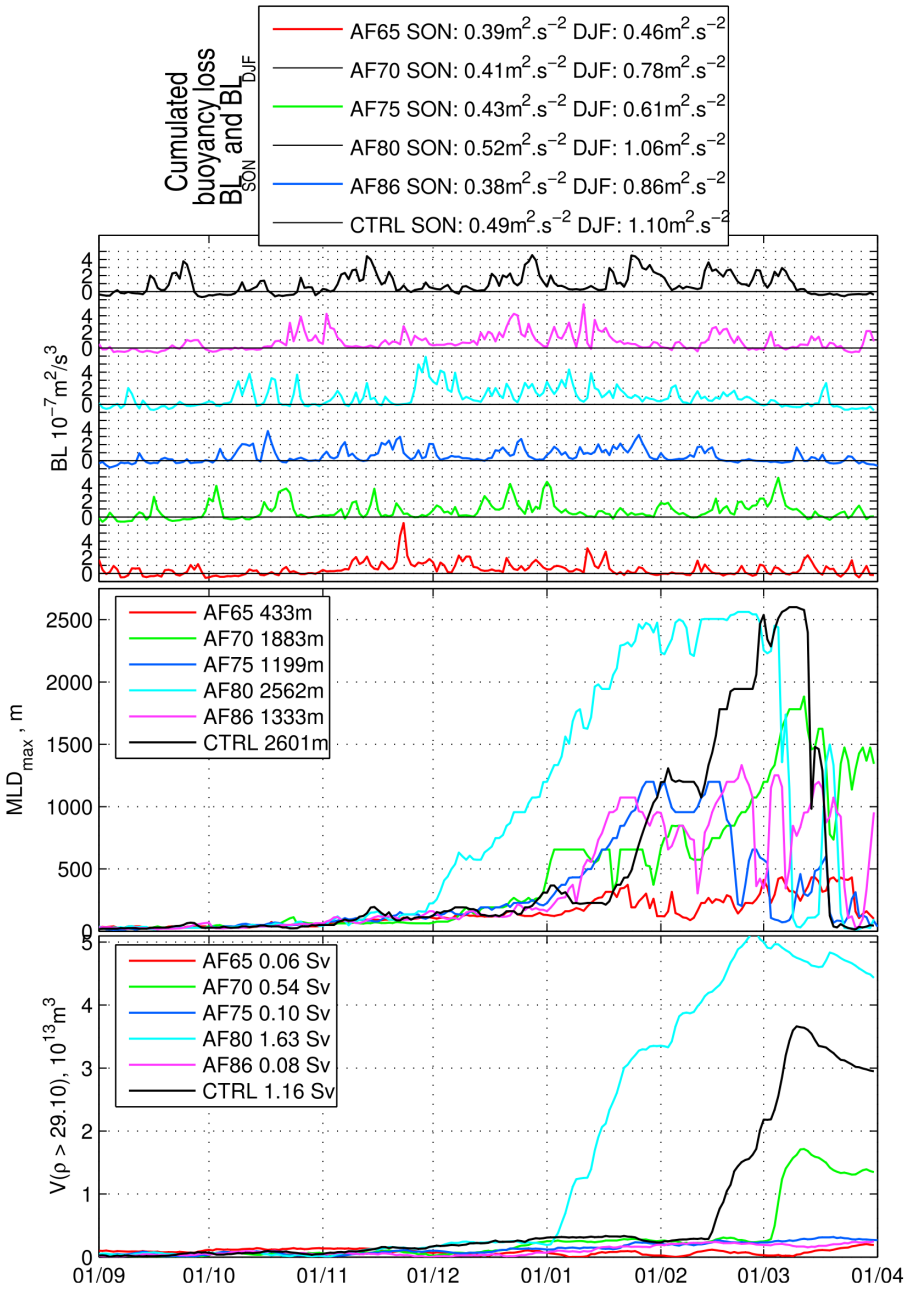

Figure 9. For simulations performed with the initial oceanic conditions of August 2004 of CTRL (AF*XX* and year 2004–2005 of CTRL), time series between September and March of the average buoyancy loss over LION, *BL*; of the maximum MLD over LION, $MLD_{\max}$; and of the volume of newly formed WMDW, V_{DW}. For each simulation we indicate the values of (top) the buoyancy loss cumulated over September–November and December–February, of (middle) the maximum of $MLD_{\max}$, and of (bottom) the WMDW formation rate.

the autumn atmospheric buoyancy loss before this phase, i. e., during the preconditioning phase [*Marshall and Schott*, 1999], certainly also plays an important role: it participates to the weakening of the stratification of the water column. The times series of the mean atmospheric buoyancy loss over LION during September–November, December–February, and September–February are presented in Figure 2. For simulations performed with the same initial oceanic conditions, the values of the cumulated buoyancy loss during those periods, BL_{SON}, BL_{DJF} and BL_{SONDJF}, are reported in Figure 9 (top). The results suggest that an atmospheric buoyancy loss stronger than the average is necessary both during the preconditioning and during the violent mixing in order to produce deep convection. In particular, in CTRL and AF80, i.e., the two simulations where convection reaches the bottom, buoyancy losses are significantly stronger than the average over 1960–2006 (BL_{SON} is equal to 0.49 and 0.52 m^2 s^{-2} in CTRL and

AF80, respectively, versus an average value of 0.48 $m^2 s^{-2}$, and BL_{DJF} is equal to 1.10 and 1.06 $m^2 s^{-2}$ versus 0.63 $m^2 s^{-2}$). On the contrary in AF65 and AF75, BL_{SON} (0.39 and 0.43 $m^2 s^{-2}$, respectively) and BL_{DJF} (0.46 and 0.61 $m^2 s^{-2}$, respectively) are both smaller than the average, and the MLD does not exceed 1500 m. However, some situations are not so straightforward: AF86 does not produce deep convection whereas AF70 does, though their values of BL_{DJF} (0.86 and 0.78 $m^2 s^{-2}$, respectively) are both larger than the average and their values of BL_{SON} (0.38 $m^2 s^{-2}$ and 0.41 $m^2 s^{-2}$, respectively) are both smaller than the average. More generally, examining the time series of the atmospheric buoyancy loss and of the maximum MLD between 1961 and 2006 in CTRL (Figure 2) shows that it is very difficult to find a clear relationship between BL and $MLD_{\max}$: see for example winters 1969–1970, 1975–1976 and 1986–1987. It would certainly be necessary to consider the influence of other factors like the frequency and duration of the atmospheric events. A much larger amount of simulations would be necessary to build a relevant indicator of atmospheric conditions to which the interannual variability of the intensity of deep convection could be related. This is, however, beyond the scope of this study, that focuses on the 2004–2005 case.

[44] Finally, our sensitivity simulations suggest that the strong atmospheric buoyancy loss observed both during autumn 2004 and winter 2004–2005, i.e., during the preconditioning and the violent mixing, was the major factor at the origin of the intensity of the convection observed this year. The particularly weak stratification of the water column in December 2004 induced by the EMT would have then accentuated the effect of this strong atmospheric conditions and potentially doubled the volume of WMDW formed, but would not have fundamentally modify the convection process.

3.3.2. Why Was the WMDW Formed in 2005 Exceptionally Warm and Salty?

[45] In this section we examine the contributions of the oceanic and atmospheric conditions before and during the convection event of 2004–2005 to the characteristics of the WMDW formed in 2005.

3.3.2.1. Impact of the Oceanic Conditions Before and During the 2004–2005 Convection Event on the WMDW Characteristics

[46] To investigate the influence of the initial oceanic conditions on the characteristics of the WMDW formed in 2004–2005, we examine the simulations where the atmospheric forcing is the one of year 2004–2005 but where the initial oceanic conditions vary: CI*XX* and year 2004–2005 of CTRL and NEMT (see section 2.3.2). For those simulations, the characteristics of WMDW formed during winter 2004–2005, corresponding to the densest water found in LION at the date of maximum convection (10 March 2005; see section 3.3.1), are indicated in Table 3 and in Figure 7b. WMDW produced in the CI*XX* simulations corresponds to old WMDW (12.73–12.82°C, 38.43–38.46; see Table 1), whereas WMDW produced in CTRL but also in NEMT corresponds to new WMDW (~12.9°C, ~38.48; see Table 1). When convection reaches the bottom, which is the case in all the simulations examined here (Figure 3), WMDW is formed by mixing of the whole water column. Therefore, we can expect the temperature and salinity of newly formed WMDW to depend on the heat and salt contents of this water column just before the convection. To confirm this hypothesis, we perform a linear regression analysis between the WMDW characteristics and the average heat and salt contents over LION on 1 December, $HC_{01/12}$ and $SC_{01/12}$ (Figures 7c and 7d). Values of $HC_{01/12}$ and $SC_{01/12}$ are reported in Table 3. T_{DW} and S_{DW} are linearly related to $HC_{01/12}$ and $SC_{01/12}$, respectively, with correlation factors larger than 0.95 (SL >0.99). The fact that WMDW produced in 2005 corresponds to old WMDW characteristics in the CI*XX* simulations and to new WMDW in CTRL suggests that the exceptional atmospheric heat and salt losses that occurred during winter 2004–2005 were not responsible for the observed change of WMDW characteristics, and that this change was rather due to the evolution of the oceanic heat and salt contents until 2004.

[47] To investigate the contribution of the oceanic lateral fluxes of heat and salt during the convection to the characteristics of the WMDW formed in 2005, we perform heat and salt budgets over LION between t_{init} = 1 December 2004 and $t \le t_{fin}$ = 31 March 2005 for simulations performed under the atmospheric forcing of 2004–2005. During this period, the variation of heat content over LION is equal to the sum of the cumulated surface and lateral fluxes of heat, and the variation of salt content is equal to the cumulated lateral flux of salt:

$$\Delta_{t_{init}-t} HC = \int_{t_{init}}^{t} HF_{lat}(t)dt + \int_{t_{init}}^{t} HF_{surf}(t)dt$$

$$\Delta_{t_{init}-t} SC = \int_{t_{init}}^{t} SF_{lat}(t)dt \qquad (4)$$

[48] Note that surface freshwater flux associated to evaporation/precipitation (see section 2.2) does not appear in this equation. Indeed, freshwater flux does not modify the total salt content over the water column: there is no flux of salt through the ocean/atmosphere boundary, neither the water that evaporates nor the rainwater contain salt. However, surface freshwater flux induces a variation of the whole volume, and therefore a concentration/dilution that results in a modification of the average salinity. Rigorously, we should relate the salinity of DW to the average salinity over the water column rather than to the total salt content. The following scale analysis shows that this is equivalent.

[49] The variation of salinity induced by a change of volume dV due to evaporation/precipitation is equal to $dS_{WF} = -S\frac{dV}{V}$. The variation of salinity induced by a variation of salt content ΔSC is equal to $dS_{HC} = \frac{\Delta SC}{\rho V}$. Among winters examined in our sensitivity simulations, deep convection occurs during winters 1970–1971, 1980–1981 and 2004–2005. Between December and February, the net freshwater flux WF_{DJF} and the initial salt content on 1 December $SC_{01/12}$, in CTRL over the surface area are equal to $WF_{DJF} \sim 3.9$ mm d^{-1} and $SC_{01/12} \sim 8.729 \times 10^7$ g m^{-2}, respectively, in 1970–1971, $WF_{DJF} \sim 3.6$ mm d^{-1} and $SC_{01/12} \sim 8.733 \times 10^7$ g m^{-2} in 1980–1981 and $WF_{DJF} \sim 4.4$ mm d^{-1} and $SC_{01/12} \sim 8.737 \times 10^7$ g m^{-2} in 2004–2005. Those values provide an estimate of the interannual variability of winter freshwater

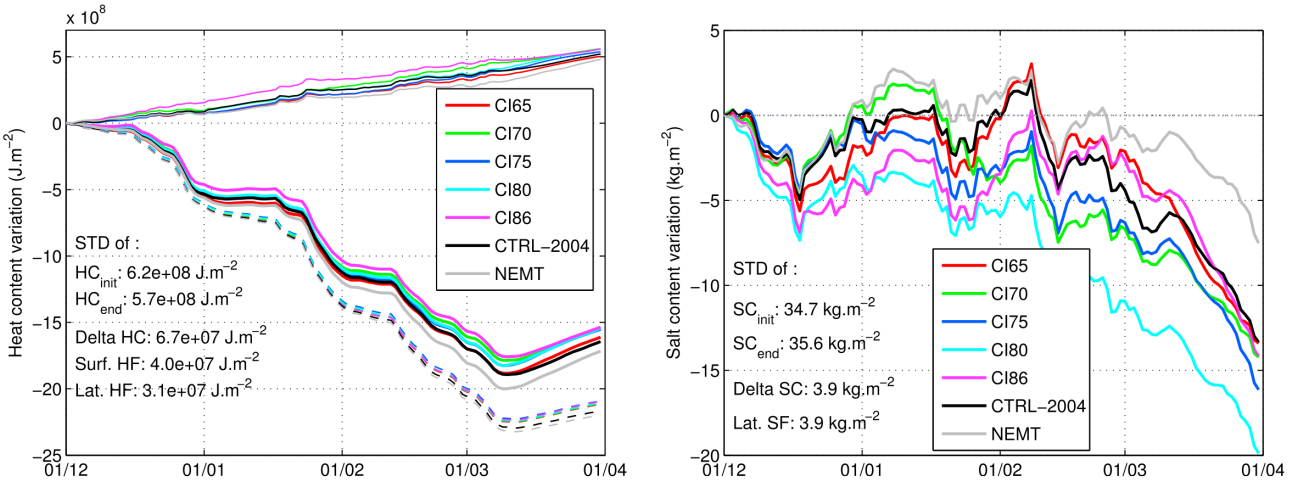

Figure 10. (left) Heat and (right) salt budgets over LION between December 2004 and March 2005 in the simulations performed under the atmospheric forcing of 2004–2005. Daily time series of the variation of the total heat and salt contents (*HC* and *SC*, bold lines), of the cumulated atmospheric heat flux (HF_{surf}, dashed lines), and of the cumulated lateral heat and salt fluxes (HF_{lat} and SF_{lat}, thin lines) since 1 December. Values of the initial contents on 1 December (HC_{init}, SC_{init}), of the final contents at the date of maximum convection, i.e., 10 March (HC_{fin}, SC_{fin}), of the variation of the heat content (Delta HC, Delta SC), of the cumulated surface heat flux (Surf. HC), and of the cumulated lateral atmospheric heat and salt fluxes (Lat. HC and Lat. SC) between 1 December and 10 March are indicated in black.

flux and initial salt content over years of deep convection. Between winters 1970–1971 or 1980–1981 and winter 2004–2005, the difference of freshwater flux is ΔWF_{DJF} = [0.5;0.8] mm d^{-1} corresponding a difference of volume of dV = [0.05;0.08] m over a period of 100 days (i.e., approximately the length of the convection period, beginning of December to mid-March). The mean height of the water column is ~2000 m. The difference of salinity induced by this difference of freshwater flux is therefore $dS_{WF} \sim 38 \times [0.05;0.08]/2000 = [0.9;1.5]10^{-3}$. Between winters 1970–1971 or 1980–1981 and winter 2004–2005, the difference of salt content is $\Delta SC_{01/12} = [40;80]10^4$ g m^{-2}. The difference of salinity induced by this difference of salt content is equal $dS_{SC} \sim [40; 80]10^4/(1029 \times 2000) = [1.9;3.9]10^{-2}$.

[50] In our model, the variation of salinity induced by the interannual variability of freshwater fluxes during the convection period is therefore ~20 times smaller than the variation of salinity associated to variability of the initial salt content, hence negligible. This justifies that we could neglect the impact of the freshwater flux on the average salinity and therefore relate the salinity of DW directly to the total salt content, and not only to the average salinity.

[51] The evolution of the terms of equation (4) are shown in Figure 10. The evolution of the variation of heat content during the convection event is very similar in each simulation, as well as the evolution of the cumulated lateral and surface heat fluxes.As a result, the contribution of those fluxes to the variability of the heat content is 1 order of magnitude smaller than the contribution of the initial heat content: the values of the standard deviation among the simulations of the total cumulated lateral and surface heat fluxes between 1 December and 10 March, when the convection is the strongest, are equal to 5×10^7 and 3×10^7 J m^{-2}, respectively, i.e., approximately 10 to 20 times smaller than the standard deviation of the initial heat content (6 10^8 J m^{-2}). Similarly, the variability of the lateral salt flux, which evolves similarly in each simulation, is much weaker than the variability of the initial salt content: the standard deviation of the total cumulated lateral salt flux is equal to 3.7 kg m^{-2}, i.e., ~10 times smaller than the standard deviation of the initial salt content (35 kg m^{-2}).

[52] Our results suggest that for given atmospheric conditions, the variability of the characteristics of the newly formed WMDW is mainly related to the variability of the initial heat and salt contents. The lateral oceanic heat and salt fluxes during the convection do not contribute significantly to the variability of these heat and salt contents, hence to the variability of the WMDW characteristics.

3.3.2.2. Impact of the Atmospheric Conditions During the 2004–2005 Convection Event on the WMDW Characteristics

[53] We showed in section 3.3.1 that the intensity of winter convection in terms of depth is mainly driven by the autumn and winter atmospheric conditions. The deeper the convection is, the larger the amount of WMDW already present in the convection area and mixed with the overlying water is. The relative proportions of WMDW and LIW contributing to the formation of new WMDW are therefore larger and smaller, respectively, when the convection is deeper. For given initial oceanic conditions, the WMDW being less warm and salty than the LIW, the temperature and salinity of the resulting newly formed WMDW will therefore be smaller for larger depths of convection. This effect can be observed in our modeling study when comparing simulations where initial oceanic conditions are identical and where atmospheric conditions are different but induce deep convection, i.e., year 1970 of CTRL with CI70, year 1980 of CTRL with CI80, and AF70, AF80 and year 2004

of CTRL: for given initial oceanic conditions, T_{DW} and S_{DW} decrease when $MLD_{\max}$ and MLD_{mean} increase (Table 3). In particular, the comparison of AF70, AF80 and year 2004 of CTRL shows that if different atmospheric conditions had occurred in 2004–2005, e.g., those of winters 1970–1971 or 1980–1981, deep convection could still have occurred ($MLD_{\max}$ = 1883 m in AF70, 2562 m in AF80 and 2601 m in CTRL) and the change of WMDW could have been even more spectacular than the change observed in reality since the mixed layer would have been slightly shallower (T_{DW} and S_{DW} are equal to 13.04°C and 38.513 in AF70 and 12.92°C, 38.488 in AF80 versus 12.90°C, 38.483 in CTRL). Another interesting point is that the characteristics of convection during winter 1980–1981 of CTRL (12.90°C, 38.479 and 29.113 kg m^{-3}) correspond to new characteristics: the conjunction of smaller heat and salt contents than those of August 2004 (1.188 10^{11} J m^{-2} and 8.733 10^4 kg m^{-2} in 1980–1981 versus 1.198 10^{11} J m^{-2} and 8.737 10^4 kg m^{-2} in 2004–2005; Figure 4 and Table 3) with smaller maximum and mean MLD (2382 m and 510 m versus 2601 m and 943 m; Table 3) led to the formation of WMDW with similar characteristics (12.90°C, 38.479 versus 12.90°C, 38.483). Finally the atmospheric conditions during the convection indirectly influence the characteristics of newly formed WMDW by determining the depth of convection.

3.3.2.3. Impact of the EMT on WMDW Characteristics

[54] Finally, the results obtained in sections 3.3.2.2 and 3.3.2.1 show that the change of temperature and salinity of the WMDW formed during winter 2004–2005 compared to the WMDW formed before was not due to the atmospheric conditions neither to the lateral oceanic advection during this winter, but to the initial heat and salt contents of autumn 2004 over LION, which were exceptionally high. We showed in section 3.1 that these high 2004 contents, obtained both in NEMT and CTRL, were not due to the EMT but to the absence of deep convection during the 1990s, itself induced by a succession of weak buoyancy loss winters. Our results therefore show that the EMT was not responsible for the change of WMDW characteristics observed during the 2005 convection episode, contrary to what was suggested by *Schroeder et al.* [2008].

[55] Note that this result explains why the simulation used by *Herrmann et al.* [2009] in order to study the interannual variability of the NWMED convection for the period 1998–2007 was not able to reproduce the change of WMDW characteristics observed in 2005. During the 10 years spin-up corresponding to the period 1987–1997, ERA40 fields were indeed used for the atmospheric forcing. Their resolution, ~125 km, is not sufficient to reproduce realistically the Mediterranean circulation and in particular the NWMED deep convection [*Herrmann and Somot*, 2008]. Consequently, this simulation could not reproduce correctly the circulation of water masses during this period in the NWMED, and therefore the salting and warming responsible for the change of WMDW characteristics observed in 2005.

4. Conclusion

[56] In this paper we focus on the exceptionally strong convection event that occurred in the NWMED during winter 2004–2005, associated with newly formed WMDW warmer and saltier than usually. Experimental oceanographers that observed this event proposed two explanations: the first one relates the exceptional intensity of this convection event, as well as the change of the characteristics of WMDW formed this winter to the atmospheric conditions. The second one relates them to the effect of the EMT on the intermediate layer of the NWMED, hence on the oceanic conditions. We used numerical modeling in order to determine which element played a role in this event, and how.

[57] We first performed a realistic numerical simulation of the Mediterranean oceanic circulation during the 1960–2006 period. The long-term analysis of this simulation was performed by *Beuvier et al.* [2010], who validated the long-term evolution of the temperature and salinity in the whole basin, and showed that the model reproduces correctly the EMT. Here we showed that this control simulation is able to reproduce realistically the 2005 NWMED convection event: the temporal and spatial evolution of the convection event as well as the WMDW characteristics were consistent with satellite and in situ observations.

[58] Sensitivity simulations then allowed us to assess the respective contributions of the oceanic and atmospheric conditions to the 2004–2005 convection event. First, we examined the factors that led to the structure of the water column in the NWMED just before the convection. Our model suggests that a succession of winters of weak atmospheric buoyancy loss was responsible for the absence of deep convection during the 1990s. This would have enabled the heat and salt to accumulate in the intermediate layer. Consequently, the heat and salt contents of autumn 2004 were the highest of the whole 1960–2005 period, in agreement with the observations of *Schroeder et al.* [2010]. According to our model, the EMT did not contribute significantly to this warming and salting of the intermediate layer, but it induced the deepening of the heat and salt maximum in the NWMED. This deepening, already observed by *Gasparini et al.* [2005], was associated with a weakening of the stratification of the water column in autumn 2004 compared to what would have been the case without the EMT.

[59] We then determined which were the key factors that could be responsible for the characteristics of the 2004–2005 convection event. In our model, the abrupt change of WMDW characteristics observed in 2005 predominantly resulted from the high heat and salt contents of autumn 2004. It therefore seems that it was not due do the EMT but to the weakness of the winter atmospheric buoyancy loss and deep convection in the NWMED during the 1990s. Moreover, our results suggest that the lateral oceanic heat and salt fluxes during winter 2004–2005 did not play a significant role in the settings of the WMDW characteristics. The atmospheric conditions of 2004–2005, namely the strong autumn and winter atmospheric buoyancy losses, mainly drove the deepening of the mixed layer in our model. They consequently appear to be the major factor responsible for the exceptional intensity of the convection observed this winter in terms of depth and volume of newly formed WMDW. The EMT would have accentuated the effect of the atmospheric forcing by weakening the stratification, hence facilitating the vertical mixing of the water column. This would have not fundamentally change the convection process and depth but potentially doubled the volume of newly formed WMDW. Finally, our conclusions were obtained using a given ocean model forced by a given atmospheric

data set. It would be necessary to perform other simulations using other models and atmospheric forcings in order enforce the robustness of our conclusions or to propose alternative explanations.

[60] In this study, we focused on winter 2004–2005 and on the NWMED in order to understand the mechanisms responsible for the spectacular convection that occurred this year. WMDW formed in 2005 then propagated into the rest of the basin [*Schroeder et al.*, 2008] and a signal apparently reached the Gibraltar Strait. *García Lafuente et al.* [2007] indeed observed a decrease of the temperature of the Mediterranean Outflow Water in March 2005 and 2006. They attributed it to a remote signature of the strong NWMED convection that occurred those winters. Our simulations could help to understand how the 2004–2005 convection event in the NWMED influenced the circulation in the rest of the basin and this motivates further studies. Our next goal is to use and perform additional realistic long-term simulations in order to quantify more generally the contributions of the oceanic and atmospheric conditions to the interannual variability of the convection characteristics, in the NWMED but also in the other regions of deep and intermediate convection of the Mediterranean Sea (Adriatic, Aegean, Levantine subbasins) and study how these local processes can interact between each other in particular through the thermohaline circulation.

[61] **Acknowledgments.** This study has been sponsored by the "Forecast and projection in climate scenario of Mediterranean intense events: Uncertainties and Propagation on environment" (MEDUP) project of the program Vulnérabilité: Milieux et Climat from the Agence Nationale pour la Recherche and by the HyMeX project (Hydrological cycle in the Mediterranean experiment (www.hymex.org)). We thank C. Millot, K. Schroeder, and an anonymous reviewer for their comments and suggestions that helped to improve the quality of this paper. We also thank D. Quoc-Phi, M. Remaud, and A. Verrelle for their work at the very beginning of this study.

References

Barnier, B., et al. (2006), Impact of partial steps and momentum advection schemes in a global ocean circulation model at eddy-permitting resolution, *Ocean Dyn.*, *56*, 543–567.

Beuvier, J., F. Sevault, M. Herrmann, H. Kontoyiannis, W. Ludwig, M. Rixen, E. Stanev, K. Béranger, and S. Somot (2010), Modeling the Mediterranean Sea interannual variability during 1961–2000: Focus on the Eastern Mediterranean Transient (EMT), *J. Geophys. Res.*, *115*, C08017, doi:10.1029/2009JC005950.

Blanke, B., and P. Delecluse (1993), Variability of the tropical Atlantic Ocean simulated by a general circulation model with two different mixed layer physics, *J. Phys. Oceanogr.*, *23*, 1363–1388.

Bozec, A., P. Bouret-Aubertot, D. Iudicone, and M. Crépon (2008), Impact of penetrative solar radiation on the diagnosis of water mass transformation in the Mediterranean Sea, *J. Geophys. Res.*, *113*, C06012, doi:10.1029/2007JC004606.

Castellari, S., N. Pinardi, and K. Leaman (2000), Simulation of water mass formation processes in the Mediterranean Sea: Influence of the time frequency of the atmospheric forcing, *J. Geophys. Res.*, *105*(C10), 24,157–24,181, doi:10.1029/2000JC900055.

CLIPPER Project Team (1999), Modélisation à haute résolution de la circulation dans l'océan Atlantique forcée et couplée océan-atmosphère, *Sci. Tech. Rep. CLIPPER-R3*-99, Lab. des Ecoulements Géophys. et Ind., Grenoble, France.

Déqué, M., and J. Piedelievre (1995), High-resolution climate simulation over Europe, *Clim. Dyn.*, *11*, 321–339.

Font, J., P. Puig, J. Salat, A. Palanques, and M. Emelianov (2007), Sequence of hydrographic changes in NW Mediterranean deep water due to the exceptional winter of 2005, *Sci. Mar.*, *71*, 339–346.

García Lafuente, J., A. Sánchez Román, G. Díaz del Río, G. Sannino, and J. C. Sánchez Garrido (2007), Recent observations of seasonal variability of the Mediterranean outflow in the Strait of Gibraltar, *J. Geophys. Res.*, *112*, C10005, doi:10.1029/2006JC003992.

Gasparini, G., A. Ortona, G. Budillon, M. Astraldi, and E. Sansone (2005), The effect of the Eastern Mediterranean Transient on the hydrographic characteristics in the Strait of Sicily and in the Tyrrhenian Sea, *Deep Sea Res., Part II*, *52*, 915–935.

Gibson, J., P. Kållberg, S. Uppala, A. Hernandez, and E. Serano (1997), ERA description, in *Re-anal*, *Proj. Rep. Ser.*, Eur. Cent. for Medium-Range Weather Forecast, Reading, U. K.

Guldberg, A., E. Kaas, M. Déqué, S. Yang, and S. Vester Thorsen (2005), Reduction of systematic errors by empirical model correction: Impact on seasonal prediction skill, *Tellus, Ser. A*, *57*, 575–588.

Herrmann, M. J., and S. Somot (2008), Relevance of ERA40 dynamical downscaling for modeling deep convection in the Mediterranean Sea, *Geophys. Res. Lett.*, *35*, L04607, doi:10.1029/2007GL032442.

Herrmann, M., S. Somot, F. Sevault, C. Estournel, and M. Déqué (2008), Modeling the deep convection in the northwestern Mediterranean sea using an eddy-permitting and an eddy-resolving model: Case study of winter 1986–1987, *J. Geophys. Res.*, *113*, C04011, doi:10.1029/2006JC003991.

Herrmann, M., J. Bouffard, and K. Béranger (2009), Monitoring open-ocean deep convection from space, *Geophys. Res. Lett.*, *36*, L03606, doi:10.1029/2008GL036422.

Kalnay, E., et al. (1996), The NCEP/NCAR 40-year reanalysis project, *Bull. Am. Meteorol. Soc.*, *77*, 437–471.

López-Jurado, J.-L., C. González-Pola, and P. Vélez-Belchí (2005), Observation of an abrupt disruption of the long-term warming trend at the Balearic Sea, western Mediterranean Sea, in summer 2005, *Geophys. Res. Lett.*, *32*, L24606, doi:10.1029/2005GL024430.

Madec, G. (2008), NEMO ocean engine, *Note Pole de Modélisation 27*, Inst. Pierre-Simon Laplace, Paris.

Marshall, J., and F. Schott (1999), Open-ocean convection: Observations, theory, and models, *Rev. Geophys.*, *37*(1), 1–64.

MEDAR/MEDATLAS Group (2002), *MEDAR/MEDATLAS* 2002 *Database: Cruise Inventory, Observed and Analysed Data of Temperature and Bio-Chemical Parameters* [4 CD-ROMs], Inst. Fr. de Rech. Pour l'Exploit. de la Mer, Brest, France.

Mertens, C., and F. Schott (1998), Interannual variability of deep-water formation in the northwestern Mediterranean, *J. Phys. Oceanogr.*, *28*, 1410–1424.

Millot, C. (1999), Circulation in the western Mediterranean Sea, *J. Mar. Syst.*, *20*, 423–442.

Millot, C. (2005), Circulation in the Mediterranean Sea: Evidences, debates and unanswered questions, *Sci. Mar.*, *69* 5–21, doi:10.3989/scimar.2005.69s15.

Perry, K. (2001), SeaWinds on QuikSCAT Level 3 Daily, Gridded Ocean Wind Vectors (JPL SeaWinds Project), http://podaac.jpl.nasa.gov/DATA_CATALOG/quikscatinfo.html, JPL Phys. Oceanogr. DAAC, Pasadena, Calif.

Reynaud, T., P. Legrand, H. Mercier, and B. Barnier (1998), A new analysis of hydrographic data in the Atlantic and its application to an inverse modeling study, *Int. World Ocean Circ. Exp. Newsl. 32*, Natl. Oceanogr. Data Cent., Silver Spring, Md.

Rixen, M., et al. (2005), The Eestern Mediterranean Deep Water: A proxy for climat change, *Geophys. Res. Lett.*, *32*, L12608, doi:10.1029/2005GL022702.

Roether, W., B. Klein, B. Manca, A. Theocharis, and S. Kioroglou (2007), Transient eastern Mediterranean deep waters in response to the massive dense-water output of the Aegean Sea in the 1990s, *Prog. Oceanogr.*, *74*, 540–571.

Salat, J., M. Emelianov, and J. López-Jurado (2006), Unusual extension of western Mediterranean deep water formation during winter 2005, paper presented at 5 Asamblea Hispano-Portuguesa de Geodesia y Geofisica, Minist. de Medio Ambiente, Sevilla, Spain.

Sannino, G., M. Herrmann, A. Carillo, V. Rupolo, V. Ruggiero, V. Artale, and P. Heimbach (2009), An eddy-permitting model of the Mediterranean Sea with a two-way grid refinement at the Strait of Gibraltar, *Ocean Modell.*, *30*, 56–72, doi:10.1016/j.ocemod.2009.06.002.

Schröder, K., G. P. Gasparini, M. Tangherlini, and M. Astraldi (2006), Deep and intermediate water in the western Mediterranean under the influence of the Eastern Mediterranean Transient, *Geophys. Res. Lett.*, *33*, L21607, doi:10.1029/2006GL027121.

Schroeder, K., A. Ribotti, M. Borghini, R. Sorgente, A. Perilli, and G. P. Gasparini (2008), An extensive Western Mediterranean Deep Water renewal between 2004 and 2006, *Geophys. Res. Lett.*, *35*, L18605, doi:10.1029/2008GL035146.

Schroeder, K., S. A. Josey, M. Herrmann, L. Grignon, G. P. Gasparini, and H. L. Bryden (2010), Abrupt warming and salting of the Western Med-

iterranean Deep Water: Atmospheric forcings and lateral advection, *J. Geophys. Res.*, *115*, C08029, doi:10.1029/2009JC005749.

Sevault, F., S. Somot, and J. Beuvier (2009), A regional version of the NEMO ocean engine on the Mediterranean Sea: NEMOMED8 user's guide, *Note Cent. 107*, Groupe de Météorol. de Grande Echelle et Climat, CNRM, Toulouse, France.

Smith, R. O., H. L. Bryden, and K. Stansfield (2008), Observations of new Western Mediterranean Deep Water formation using Argo floats 2004–2006, *Ocean Sci.*, *4*, 133–149.

Smith, W., and D. Sandwell (1997), Global sea floor topography from satellite altimetry and ship depth sounding, *Science*, *277*(5334), 1956–1962.

Somot, S., F. Sevault, and M. Déqué (2006), Transient climate change scenario simulation of the Mediterranean Sea for the twenty-first century using a high-resolution ocean circulation model, *Clim. Dyn.*, *27*, 851–579, doi:10.1007/s00382-006-0167-z.

Stanev, E., P.-Y. Le Traon, and E. Peneva (2000), Sea level variations and their dependency on meteorological and hydrological forcing: Analysis of altimeter and surface data for the Black Sea, *J. Geophys. Res.*, *105*(C7), 17,203–17,216.

Testor, P., and J.-C. Gascard (2006), Post-convection spreading phase in the northwestern Mediterranean Sea, *Deep Sea Res., Part I*, *53*, 869–893.

Vörösmarty, C., B. Fekete, and B. Tucker (1996), *Global River Discharge Database* (*RivDis*), *Int. Hydrol. Program*, Global Hydrol. Archive and Anal. Syst., UNESCO, Paris.

J. Beuvier, ENSTA-ParisTech/UME, Chemin de la Hunière, F-91761 Palaiseau CEDEX, France.

M. Herrmann, F. Sevault, and S. Somot, CNRM-GAME, Météo-France/CNRS, 42 Av. Gaspard Coriolis, F-31057 Toulouse CEDEX, France. (marine.herrmann@m4x.org)

Annexe B

Version révisée de l'article de la section 5.1

Dans cette version révisée de l'article *Beuvier et al.* (en révision), la simulation MED12-ARPERA mentionnée correspond à la simulation MED12-ARPERA-3 de ce manuscrit. Suivant les commentaires anonymes des reviewers de cet article, nous avons concentré l'étude sur cette seule simulation ; les simulations MED12-ARPERA-1 et MED12-ARPERA-2 de la version initiale ne sont donc plus mentionnées dans cette version révisée.

Beuvier, J., K. Béranger, C. Lebeaupin Brossier, S. Somot, F. Sevault, Y. Drillet, R. Bourdallé-Badie, N. Ferry, and F. Lyard (en révision), Spreading of the Western Mediterranean Deep Water after winter 2005 : time-scales and deep cyclone transport, *Journal of Geophysical Research*, in revision.

Résumé

Ce travail est consacré à l'étude de la propagation de l'eau ouest-méditerranéenne profonde (*Western Mediterranean Deep Water*, WMDW) formée dans le Golfe du Lion au cours de l'hiver exceptionnel de 2005. Des simulations de la période 1998-2008 ont été réalisées avec un modèle de circulation générale océanique "eddy-resolving" de la mer Méditerranée, forcé par des flux air-mer interannuels et à haute résolution. Cette étude présente tout d'abord une validation des améliorations récentes de la configuration du modèle, face à des observations satellites. Puis, nous évaluons la capacité du modèle à reproduire l'évenement de convection profonde particulièrement intense dans le Golfe du Lion pendant l'hiver 2005. Un volume conséquent d'eau très dense est formé dans les simulations à cette date (taux de formation annuel d'environ 3 Sv). Les caractéristiques thermohalines de la nouvelle WMDW permette de suivre sa propagation en profondeur. Nous identifions plusieurs cyclones profonds comme étant principalement responsables de la propagation rapide de la WMDW vers le Sud dans le bassin occidental de la Méditerranée. En comparant des approches eulériennes et lagrangiennes, nous estimons différents temps de transport de la WMDW par ces tourbillons cycloniques et nous les comparons à ceux déduits des observations. Finalement, nous affirmons que ces cyclones favorisent la propagation des caractéristiques thermohalines de la WMDW vers le canal de Sardaigne et qu'ils diminuent le volume de WMDW qui peut atteindre le détroit de Gibraltar.

Spreading of the Western Mediterranean Deep Water after winter 2005 : time-scales and deep cyclone transport

J. Beuvier, K. Béranger, C. Lebeaupin Brossier, S. Somot, F. Sevault, Y. Drillet, R. Bourdallé-Badie, N. Ferry, F. Lyard, *Journal of Geophysical Research*, in revision.

Abstract

This work is dedicated to the study of the propagation of the Western Mediterranean Deep Water (WMDW) formed in the Gulf of Lions during the exceptional winter 2005. Simulations of the 1998-2008 period have been carried out with an eddy-resolving Ocean General Circulation Model of the Mediterranean Sea, driven by interannual high-resolution air-sea fluxes. This study first presents a validation of the recently improved model configuration against satellite observations. Then, we assess the ability of the model to reproduce the particularly intense deep convection event of winter 2005 in the Gulf of Lions. A huge volume of very dense water is formed in the simulations at that time (annual formation rate of about 3 Sv). The thermohaline characteristics of the new WMDW allow a monitoring of its deep propagation. We identify several deep cyclones as mainly responsible of the fast spreading of the WMDW southwards in the Western Mediterranean. By comparing Eulerian and Lagrangian approaches, we estimate different transport times of the WMDW by these cyclonic eddies and compare them to those deduced from several observations. Finally, we argue that these cyclones favour the propagation of the WMDW thermohaline characteristics towards the Channel of Sardinia and decrease the volume of WMDW which can reach the Strait of Gibraltar.

B.1 Introduction

Deep convection occurs in the Mediterranean Sea, in particular in the Gulf of Lions in the Western Mediterranean (GoL in Fig.1). In this particular place, the formation of deep water is mainly triggered by the atmosphere with strong local winds, which lead to a high latent heat loss for the sea (*Schott et al.*, 1996), and by a topographic control (*Madec et al.*, 1996). The formation process was well described by *Marshall and Schott* (1999) in three phases : the preconditionning, the convection and the spreading. The particular circulation through a cyclonic gyre in the Gulf of Lions is enhanced in winter by the winds channeled by the Alps, the Massif Central and the Pyrenees. In the center of this relatively closed gyre, above which strong heat loss occurs, is formed the Western Mediterranean Deep Water (WMDW) in winter. The WMDW plays a major role in the thermohaline circulation of the Mediterranean. This water mass is characterised by a density above 29.10 $kg.m^{-3}$ (*MEDOC Group*, 1970). The convection regularly reaches the sea bottom, which is about 2400 m depth in this area, and occurs around the 42 °N - 5 °E position, as observed for example in 1982 (*THETIS Group*, 1994).

High resolution ocean modelling studies have proved their skill to accurately reproduce the convection process, at basin scale (*Pinardi and Masetti*, 2000; *Castellari et al.*, 2000; *Artale et al.*, 2002; *Béranger et al.*, 2005; *Fernàndez et al.*, 2005; *Somot et al.*, 2006; *Sannino et al.*, 2009; *Beuvier et al.*, 2010b; *Herrmann et al.*, 2010) or at regional scale in embedded models (*Mantziafou and Lascaratos*, 2004; *Herrmann and Somot*, 2008; *Herrmann et al.*, 2008). In these modelling studies, the atmospheric resolution was proved to be of high importance to allow the simulation of the deep convection without some artificial added forcings. In particular, the wind channeling is one of the main factor that helps the preconditionning phase (*Béranger et al.*, 2010), in producing extreme heat loss (*Herrmann and Somot*, 2008).

During the winter 2005, a drastic convection event occured in the Gulf of Lions (*López-Jurado et al.*, 2005; *Schröder et al.*, 2006; *Canals et al.*, 2006; *Font et al.*, 2007; *Smith et al.*, 2008; *Schroeder et al.*, 2008). Before the event, the previous WMDW has characteristics ranging in 12.75-12.92 °C for potential temperature, in 38.41-38.47 psu for salinity and in 29.09-29.10 $kg.m^{-3}$ for potential density (see also *Pinot et al.* (2002) and *Pascual et al.* (2002)). After the event, the new WMDW potential temperature ranges between 12.87 and 12.90 °C, and, the new WMDW salinity ranges between 38.47 and 38.50 psu. The new WMDW has thus a well marked thermohaline signature, as it is saltier and slightly warmer than the previous one, with a corresponding density range of 29.11-29.13 $kg.m^{-3}$. The formation rate of new WMDW was particularly high compared to other years. *Schroeder et al.* (2008) proposed a value of 2.4 Sv for the two winters 2005 and 2006, while previous estimates are ranged for observations between 0.1 and 1.2 Sv (*Schott et al.*, 1996; *Marshall and Schott*, 1999) and for models between 0.2 and 1.6 Sv (*Castellari et al.*, 2000; *Somot et al.*, 2006; *Béranger et al.*, 2009). An estimate of its time-scale spreading in the Western Mediterranean can be made : the new WMDW thermohaline signature was then detected in the Strait of Gibraltar (SG in Fig. 1) and in the Channel of Sardinia (CS in Fig. 1) by deep observations in 2006. *Schroeder et al.* (2008) argued that it takes less than a year and a half to this new WMDW to spread in the basin, approximately until 3 °W. But because the authors used only bi-annual sections in the basin, we do not know too much on the processes involved in this very fast spreading of new WMDW. *Testor and Gascard* (2003) and *Testor and Gascard* (2006), using Lagrangian floats during 1994-1995 and 1997-1998, have shown that submesoscale coherent vortices with a typical size of 5-10 km are one of the involved processes. They estimate that such eddies account for as much as 40% of the new WMDW spreading away from the convection area. With a coastal eddy-resolving model of the Gulf of Lions, *Herrmann et al.* (2008) have highlighted that about one third of the deep water advection after the convection event is made southwestwards by very energetic mesoscale structures with a typical size of 25-50 km.

Herrmann et al. (2010) have studied the convection phase of the winter 2005 event and its atmospheric and oceanic preconditionning factors. We here investigate the spreading phase of WMDW in winter 2005 to evaluate how the WMDW can be transported from the Gulf of Lions towards the southern channels and at what time-scale. We want to complete the fragmented view of this spreading given by the observations of *Testor and Gascard* (2003), *Testor and Gascard* (2006) and *Schroeder et al.* (2008), by using the high-resolution 4D view offered by an ocean model. We use an eddy-resolving model, described in section B.2), to study the winter 2005. The formation of WMDW during winter 2005 is first assessed in the model simulation in section B.3. Then the spreading phase is studied using eulerian and lagrangian diagnostics in section B.4. Section B.5 is devoted to a conclusion.

B.2 Model configuration and simulation

We use the ocean general circulation model NEMO (*Madec and the NEMO Team*, 2008) in a regional configuration of the Mediterranean Sea called MED12 (*Lebeaupin Brossier et al.*, 2011, 2012). The development of MED12 is made in the continuity of the evolution of the French modelling of the Mediterranean Sea, following OPAMED16 (*Béranger et al.*, 2005), OPAMED8 (*Somot et al.*, 2006) and NEMOMED8 (*Beuvier et al.*, 2010b). We described here the configuration of the 10-year simulation, named MED12-ARPERA, which will be used in this study.

B.2.1 Grid and bathymetry

MED12 covers the whole Mediterranean Sea plus a buffer zone including a part of the near Atlantic Ocean (Figure B.1). It does not cover the Black Sea. The horizontal grid of MED12 comes from the ORCA grid of NEMO at $1/12\,^\circ$ horizontal resolution for the equatorial areas. This grid corresponds in the Mediterranean Sea to a grid cell size between 6 and 8 km, from 46 °N to 30 °N (*i.e.* equivalent to a real resolution between $1/14\,^\circ$ and $1/18\,^\circ$, from South to North).

MED12 has 50 vertical stretched z-levels (from $\Delta z = 1$ m at the surface to $\Delta z = 450$ m at the

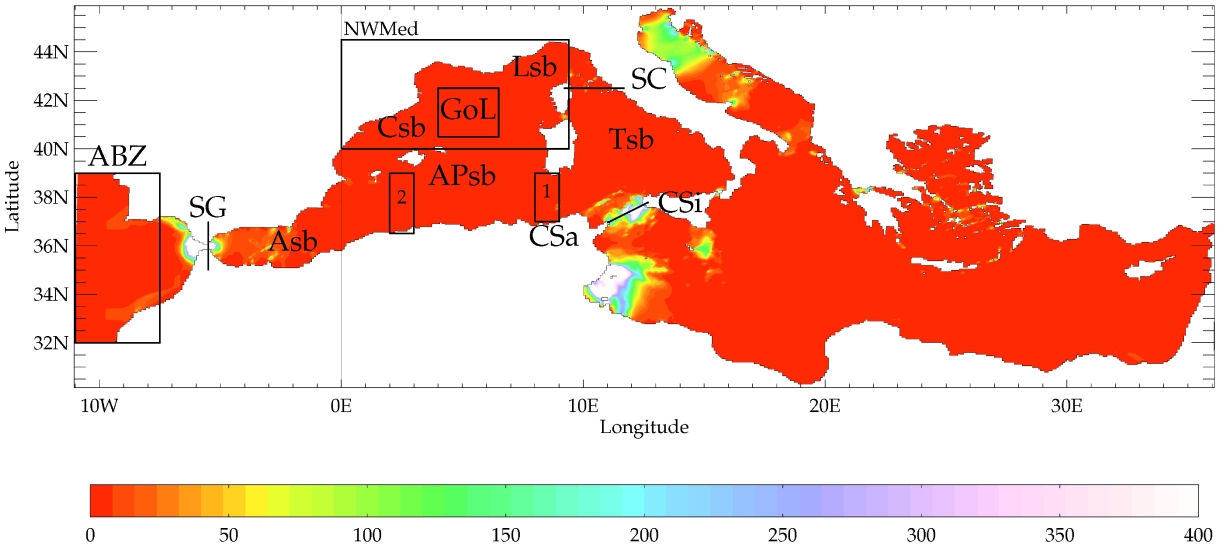

FIG. B.1 – *The domain of the MED12 model is illustrated by the bottom turbulent kinetic energy background E ($cm^2.s^{-2}$). This field has a maximum value over 10000 $cm^2.s^{-2}$ at the Strait of Gibraltar. ABZ : Atlantic Buffer Zone, SG : Strait of Gibraltar, CSa : Channel of Sardinia, CSi : Channel of Sicily, SC : Strait of Corsica, GoL : Gulf of Lions, Asb : Alboran subbasin, APsb : Algero-Provencal subbasin, Csb : Catalan subbasin, Lsb : Ligurian subbasin and Tsb : Tyrrhenian subbasin. The Algerian subbasin, when mentionned in the text, corresponds to the southern part of APsb. The rectangle in the north-western Mediterranean is the area where SSH is averaged in section B.3.2. The rectangle in the Gulf of Lions is the area where the density profiles are averaged in section B.3.3. The rectangles 1 and 2 are the boxes of the θ-S diagrams in section B.4.2.*

bottom, with 35 levels in the first 1000 m). The bathymetry comes from the 10^{th} version of the MERCATOR-LEGOS bathymetry at a resolution of 30" $\times$ 30", composed of merging between the GEBCO-08 database, the MEDIMAP bathymetry (*Medimap Group*, 2005) and the Ifremer bathymetry of the Gulf of Lions (*Berné et al.*, 2004) . We use a partial cell parameterization, i.e. the bottom layer thickness is varying to fit the real bathymetry.

B.2.2 Physics parameterizations

A time step of 12 minutes is used. The horizontal eddy diffusivity coefficient is set to 60 $m^2.s^{-1}$ for the tracers (temperature, salinity) using a laplacian operator (the diffusion is applied along iso-neutral surfaces for the tracers) and the horizontal viscosity coefficient is set to -1.25×10^{10} $m^4.s^{-2}$ for the dynamics (velocity) using of a biharmonic operator. The TVD (Total Variance Dissipation) scheme is used for the tracer advection and the EEN (Energy and

ENstrophy conservative) scheme is used for the momentum advection (*Arakawa and Lamb*, 1981; *Barnier et al.*, 2006). A 1.5 turbulent closure scheme is used for the vertical eddy diffusivity (*Blanke and Delecluse*, 1993), with an enhancement of the vertical diffusivity coefficient up to $10\,m^2.s^{-1}$ in case of unstable stratification. The solar radiation can penetrate into the ocean surface layers (*Bozec et al.* (2008)). A no-slip lateral boundary condition is used. The evolution of the sea surface is parameterised by a filtered free-surface (*Roullet and Madec*, 2000). The conservation of the model volume is assumed (see section B.2.4). The Sea Surface Height (SSH) is a prognostic variable.
The parameterization of the bottom friction $\overrightarrow{F}$ is defined as follows in NEMO :

$$\overrightarrow{F} = C_D \sqrt{U_H^2 + V_H^2 + E}\, \overrightarrow{U_H}$$

with C_D the bottom drag coefficient, U_H and V_H respectively the zonal and meridian velocities of the bottom layer, $\overrightarrow{U_H}$ the horizontal bottom speed vector and E the bottom turbulent kinetic energy background. In the simulation MED12-ARPERA, E is a 2D field (Figure B.1), corresponding to the mean tidal energy computed from a tidal model (*Lyard et al.*, 2006). The mean tidal energy is the highest in the Strait of Gibraltar (maximum value over $10000\,cm^2.s^{-2}$) and has significant values mainly in the Channel of Sicily, in the Gulf of Gabes and in the northern Adriatic Sea.

B.2.3 Initial conditions in the Mediterranean domain

For the Mediterranean Sea, the initial conditions are provided by the monthly mean potential temperature and salinity 3D fields from the MEDATLAS-II climatology (*MEDAR/MEDATLAS Group*, 2002) corresponding to October. These fields are ponderated by a low pass filtering with a time-window of three years using the MEDATLAS data covering the 1997-1999 period. The simulation then starts with initial conditions close to the Mediterranean Sea state of October 1998 and an ocean at rest.

B.2.4 Atlantic boundary conditions

The exchanges with the Atlantic ocean are performed through a buffer zone. From 11 °W to 7.5 °W (ABZ in Figure 1), 3D temperature and salinity of MED12 are relaxed towards the θ-S climatological fields of *Levitus et al.* (2005). The restoring term is weak west of Cadiz and Gibraltar area ($\tau = 90$ days at 7.5 °W) and increases westwards ($\tau = 2$ days at 11 °W).
The Mediterranean Sea is known as a basin of net evaporation compensated by the Atlantic inflow. According to the NEMO filtered free sea surface parameterization, only the volume of the first level of the model can change but the total volume of the model is not conserved, which requires thus a parameterization to do so. In previous Mediterranean configurations ($e.g.$ *Tonani et al.* (2008) or *Beuvier et al.* (2010b)), at each time-step, the water volume corresponding to the net evaporation averaged over the Mediterranean Sea (east of Gibraltar) was redistributed in the Atlantic area between 11 °W and 7.5 °W, as an input of precipitation. In MED12-ARPERA simulation, a new parameterization is implemented. The model volume is conserved through a damping of the SSH between 11 °W and 7.5 °W towards a prescribed SSH. We apply a very strong restoring, since its time scale is set to 2 seconds. The reference SSH was built by adding the mean SSH spatial pattern of a previous companion simulation with monthly sea level anomalies. For the period 2002-2008 (Figure B.2a), the anomalies are taken from GLORYS-1

(*Ferry et al.*, 2010), a reanalysis of the global ocean circulation at a $1/4^\circ$ horizontal resolution available for this period. For the period 1998-2001, the anomalies are taken from the SSH monthly cycle of the previous companion simulation with a time shift of 5 months in the seasonal cycle to follow the cycle of GLORYS-1 (Figure B.2b). We expect from this SSH restoring in the Atlantic buffer zone to constrain the horizontal pressure gradients at the entrance of the Strait of Gibraltar.

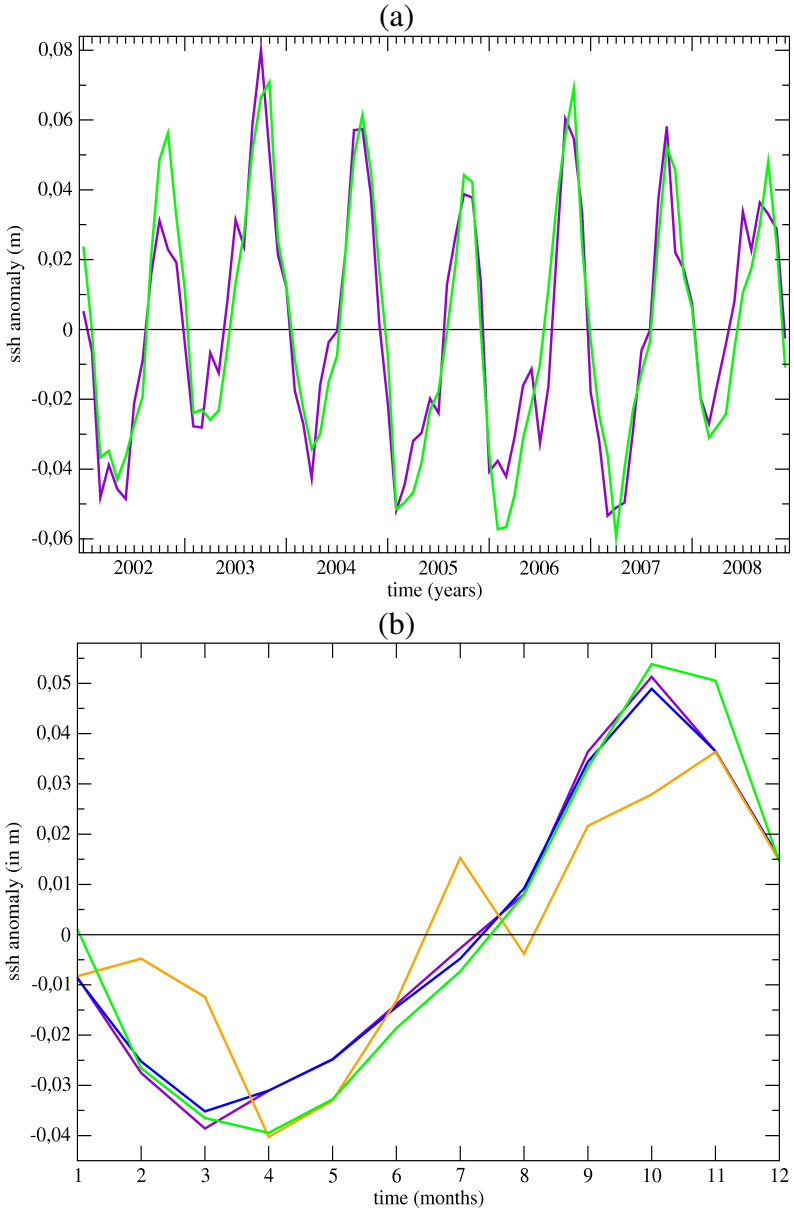

FIG. B.2 – *Monthly Sea Surface Height anomaly (m) averaged over the area [11-7.5°W, 32-39°N] (ABZ in Figure B.1) calculated by substracting the 2002-2008 SSH mean for each dataset :*
(a) for the period 2002-2008, interannual (84 monthly) values of (purple) GLORYS-1 are compared to (green) AVISO.
(b) in average for the period 2002-2008, monthly climatological values are compared between datasets : (blue) MED12-ARPERA, (purple) GLORYS-1 and (green) AVISO. In orange is added the climatological anomalies of SSH which are used in MED12-ARPERA during the 1998-2001 period.

GLORYS-1 anomalies have an amplitude of about 14 cm, in agreement with AVISO products (*Rio et al.*, 2007) which were assimilated in it (Figure B.2a). During the 2002-2008 period, the correlation between these two times-series (84 monthly values) is 0.94 . The amplitude of the interannual variations are of the order of 2 to 4 cm in both products. The AVISO products used here are the weekly Maps of Absolute Dynamic Topography (MADT), equivalent to the SSH from an oceanic model. These MADTs are built by adding weekly satellite Sea Level Anomalies (SLA) to a reference Mean Dynamic Topography (MDT).

B.2.5 River runoff and Black Sea inputs

River inputs are introduced as surface freshwater gain at the river mouths. We use the climatological average of the interannual dataset of *Ludwig et al.* (2009) to compute monthly runoff values, split in two parts. First, for the 33 main Mediterranean rivers listed in the RivDis database (*Vörösmarty et al.*, 1996), we directly take the values of the database. Second, the values of the inputs of the other rivers are gathered and averaged in each Mediterranean subbasin (as defined in *Ludwig et al.* (2009)) and put as a coastal runoff in each MED12 coastal grid point of these subbasins. These two types of river inputs contribute for the annual surface freshwater budget of the Mediterranean Sea to $+0.09\,\mathrm{m.yr^{-1}}$ for the 33 main rivers and to $+0.05\,\mathrm{m.yr^{-1}}$ for the others, $i.e.$ $+0.14\,\mathrm{m.yr^{-1}}$ in total, which is in good agreement with the $+0.14\,\mathrm{m.yr^{-1}}$ estimate of *Boukthir and Barnier* (2000) and higher than the $+0.10\,\mathrm{m.yr^{-1}}$ estimate of *Mariotti et al.* (2002).

The Black Sea is not included in MED12 but is one of the major freshwater sources of the Mediterranean Sea. The exchanges between the Black Sea and the Aegean Sea consist of a two-layer flow across the Marmara Sea and the Dardanelles Strait. We assume that this flow can be approximated by a freshwater flux diluting the salinity of the mouth grid point. Thus, in the model, the Black Sea is considered as a river for the Aegean Sea, as done in *Beuvier et al.* (2010b). We use the climatological average of the interannual dataset of *Stanev and Peneva* (2002) to compute monthly values of the Black Sea net water inflow. The annual average of this input corresponds for the surface freshwater budget of the Mediterranean Sea to $+0.10\,\mathrm{m.yr^{-1}}$.

The total freshwater input from river and Black Sea runoff amounts thus in our configuration to $+0.24\,\mathrm{m.yr^{-1}}$.

B.2.6 Atmospheric forcing

The atmospheric forcing is ARPERA, obtained by performing a dynamical downscaling of ECMWF products above the European-Mediterranean region (*Herrmann and Somot*, 2008). The downscaling method used here is a spectral nudging : it uses the atmospheric model ARPEGE-Climate (*Déqué and Piedelievre* (1995), grid streched over the Mediterranean Sea, resolution of 50 km), in which large scales (above 250 km) are spectrally driven by ECMWF fields and small scales (below 250 km) can develop freely. This dataset has a realistic synoptic chronology thanks to ECMWF fields and high-resolution structures thanks to the atmospheric resolution of ARPEGE-Climate. The simulated period lasts from the 1^{st} October 1998 to the 31^{st} December 2008. For the period 1998-2001, the driven fields come from the ERA40 reanalysis (*Simmons and Gibson*, 2000). From 2002 to 2008, fields of the ECMWF analyses are used, their resolution ($0.5\,^\circ \sim 55$ km) being downgraded to the ERA40 resolution ($1.125\,^\circ \sim 125$ km) to insure consistency between the 1998-2001 and 2002-2008 periods. ARPERA follows the real atmospheric chronology and is relevant to model realistically deep convection (*Beuvier et al.*, 2010b; *Herrmann et al.*, 2010). MED12 is forced by ARPERA daily fields of the momentum, freshwater and heat fluxes.

For the surface temperature condition, a relaxation term toward ERA40 Sea Surface Temperature (SST) is applied for the heat flux. This term actually plays the role of a first-order coupling between the SST of the ocean model and the atmospheric heat flux (*Barnier et al.*, 1995), ensuring the consistency between those two terms. The value of the relaxation coefficient is spatially constant and taken equal to $-40\,W.m^{-2}.K^{-1}$, following *CLIPPER Project Team* (1999). It is equivalent to a 1.2-day restoring time scale for a surface layer of 1 m thickness.

For the salinity surface boundary condition, no salinity damping is applied. Following *Beuvier et al.* (2010b), we add to the surface freshwater flux (E−P−R) a correction term, spatially constant, with a monthly cycle and equivalent in annual average to -0.0083 mm.d^{-1} (-0.003 m.yr^{-1}), which is neglectable with respect to the total freshwater budget. These monthly values have been computed by averaging the Sea Surface Salinity (SSS) relaxation term through a previous companion simulation with MED12 and the same atmospheric forcing. The surface freshwater budget is thus balanced without altering the spatial and temporal variations of the freshwater flux and so of the SSS. This correction term is added to the water fluxes coming from the atmospheric fields and from the rivers and Black Sea runoff. We note that the total freshwater loss (P+R−E+correction= -0.53 m.yr^{-1} for the 2002-2008 period over the Mediterranean Sea) is in the range of observations and other modelling studies (*Sanchez-Gomez et al.*, 2011).

B.3 Global validation of the circulation in the Western Mediterranean

In this section, we focus on the Western Mediterranean and on the winter 2005. After a validation of the mean and interannual behaviour of the simulation, we describe the general features of temperature, salinity, and the deep convection in the Gulf of Lions, in particular in winter 2005.

B.3.1 Exchanges through the Strait of Gibraltar

	Water flux (Sv)	Heat flux (W.m^{-2})	Salt flux (10^{-3} psu.yr^{-1})
Inflow	+0.73 $\pm$ 0.04	+20.62 $\pm$ 1.05	+218 $\pm$ 11
Outflow	-0.69 $\pm$ 0.04	-14.51 $\pm$ 0.74	-217 $\pm$ 11
Net	+0.045 $\pm$ 0.006	+6.11 $\pm$ 0.33	+1.8 $\pm$ 1.6

TAB. B.1 – *10-year averages and standard deviations of the inflowing, outflowing and net fluxes towards the Mediterranean Sea through the Strait of Gibraltar : water flux (in Sv), heat flux (in W.m^{-2}) and salt flux (in 10^{-3} psu.yr^{-1}) .*

The 10-year averages and standard deviations of the in, out and net flows of water, heat and salt in the simulation are given in Table B.1. The values for the mean water fluxes, +0.73 Sv, -0.69 Sv and +0.045 Sv respectively for the in, out and net flows, are in the lower part of the range given in the literature : between +0.72 and +1.01 Sv for the inflow, between -0.68 and -0.97 Sv for the outflow and between +0.04 and +0.13 Sv for the net flow (*Bryden and Kinder*, 1991; *Bryden et al.*, 1994; *Tsimplis and Bryden*, 2000; *Candela*, 2001; *Baschek et al.*, 2001; *Lafuente et al.*, 2002). The interannual variations for such a short period, $\pm$0.006 Sv in the simulation, are in agreement with *Soto-Navarro et al.* (2010), who estimate the water outflow during the 2004-2009 period with currentmeter observations. They give values of +0.81$\pm$0.06 Sv for the water

inflow, -0.78±0.05 Sv for the water outflow and +0.038±0.007 Sv for the net water flow. For the mean net heat flux, the value of +6.1 W.m^{-2} in the simulation is in the range of the estimations of *Béthoux* (1979) ([4 ; 10] W.m^{-2}) and of *Macdonald et al.* (1994) ([3.9 ; 6.5] W.m^{-2}). For the net salt flux, the value corresponds to the trend of the Mediterranean salt content in the simulation, and in thus quite small (+1.8 10^{-2} psu in 10 years).

B.3.2 Modelling the SSH variability

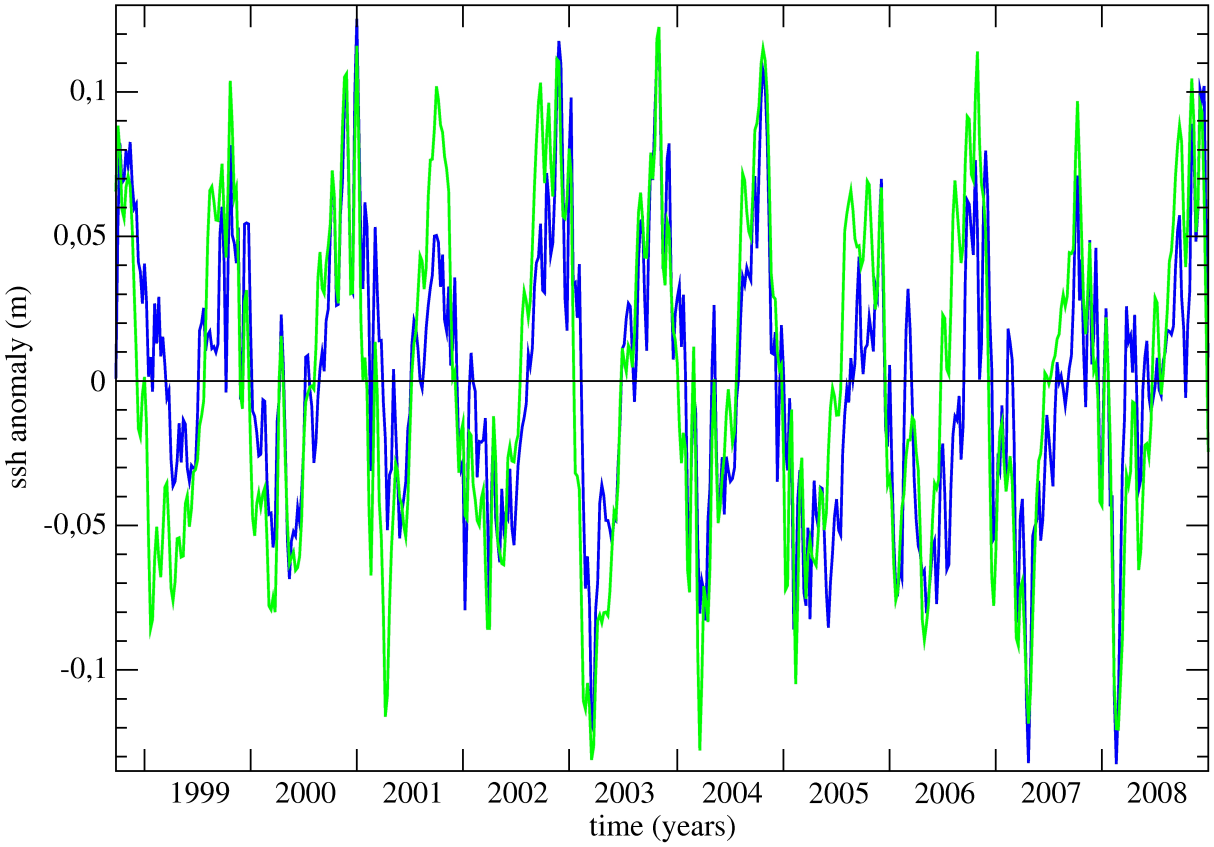

FIG. B.3 – *Weekly SSH anomalies (m) averaged over the Mediterranean Sea during the 10-year studied period for (blue) MED12-ARPERA and (green) AVISO. For each dataset, anomalies are computed around the average from October 1998 to December 2008.*

To estimate the impact of the SSH restoring in the Atlantic area applied in MED12-ARPERA, we first look, in Figure B.3, at the SSH averages over the Mediterranean Sea for the simulation and at AVISO data, produced by Ssalto/Duacs with support from CNES. We use weekly Mediterranean fields of MADT (Maps of Absolute Dynamic Topography), resulting from the sum of the SLA (Sea Level Anomalies) and of the the MDT (Mean Dynamic Topography) RioMed 2007 (*Rio et al.*, 2007) ; these data are produced in delayed time, up-to-date and merged modes. We also use the derived geostrophic currents. As the global steric signal is introduced in the model via the SSH damping in the Atlantic bufferzone to the total SSH anomalies from a global reanalysis, we do not add in our comparison the local steric effect in the Mediterranean SSH of the simulation. The peak-to-peak amplitude of the SSH variations in MED12-ARPERA (26 cm) are of the order of those of AVISO. The correlation between AVISO and MED12-ARPERA time-series (computed with the 536 de-trended weekly values) is 0.83. This agreement is explained by the better physical consistance of a SSH damping in MED12-ARPERA than the one

of the water redistribution done in previous Mediterranean oceanic configurations. In reality, the water evaporated over the Mediterranean Sea does not go back instantaneously in the ocean, and moreover it does not go all in the near Atlantic ocean. Thus, the seasonal cycle of the near Atlantic sea level in simulations with a water volume transfert is the seasonal cycle of the Mediterranean freshwater budget, which has no physical sense. By doing a SSH restoring in the buffer zone, we apply there the seasonal cycle of the water mass in this area, which explains the better agreement with sea level observations in MED12-ARPERA. The amplitude of the Mediterranean SSH is also in better agreement for simulation MED12-ARPERA thanks to the good amplitude of the prescribed SSH in the Atlantic buffer zone, which contains the effect of the steric and mass variations at global scales.

The Figure B.4 then illustrates the ability of MED12-ARPERA to reproduce the time-space variability of the SSH and of the surface currents in the Western Mediterranean Sea, in average over the 2004-2008 period. First, comparing Figure B.4a and B.4c shows that MED12-ARPERA reproduces the mesoscale variability in the Alboran and Algerian subbasins, with values of SSH RMS (Root Mean Square) corresponding to those from AVISO (between 10 and 14 cm). In the Tyrrhenian subbasin, the simulation slightly underestimates the SSH RMS but reproduces an area with high variability east off the coasts of Sardinia, near the Bonifacio eddy (*Millot and Taupier-Letage*, 2005b). In the north-western Mediterranean, the variability of the sea surface height is still lower in the simulation than in AVISO. MED12-ARPERA nevertheless reproduces higher SSH RMS in the Catalan subbasin, as in the observations. Second, we compare the EKE (Eddy Kinetic Energy) of the geostrophic currents from AVISO to the EKE of the MED12-AREPRA currents under the Ekman layer (we take these currents at about 35m depth). In the Algerian Current area, MED12-ARPERA shows higher eddy circulation, up to an EKE of $500\,cm^2.s^{-2}$, than in AVISO, which gives EKE up to $300\,cm^2.s^{-2}$, and $350\,cm^2.s^{-2}$ in the Eastern Alboran Eddy (as named by *Vargas-Yáñez et al.* (2002)). Elsewhere in the Western Mediterranean, the mean EKE value in the simulation is lower than in AVISO but shows more spatial variability, due to the higher space-time resolution of MED12-ARPERA (6-8 km for daily outputs) if compared to the resolution of AVISO products (10 km for weekly data).

In the following sections, we will focus on the dense water formation in the Gulf of Lions during winter 2005. We thus compare the surface circulation in February 2005 in the western Mediterranean for MED12-ARPERA and AVISO (Figure B.5). The main patterns of the circulation are well reproduced for this month. The surface circulation is cyclonic with the AW which enters the Mediterranean Sea through the Strait of Gibraltar. The two anti-cyclonic gyres in the Alboran Sea are present, even if their locations differ a little between the model and the observations. Then the shallow Algerian Current flows eastwards along the African coast and anticyclonic eddies more or less detached from the coast are depicted. Anticyclonic areas near 2 °E and 6 °E at around 38 °N are in agreement in both products. The Algerian Current crosses then the Channel of Sardinia and splits in several branches at the level of the Channel of Sicily. One branch enters the Tyrrhenian subbasin and circulates along the Italian coast before crossing the Strait of Corsica, generating there part of the Northern Current. This current then partly retroflects near 4 °E to form the cyclonic gyre of the Gulf of Lions, well marked in February 2005. It is centered near 42 °N - 4 °E in the model and near 41.5 °N - 6 °E in the observations. The SSH in the gyre of the Gulf of Lions is of the order and lower than $-20\,cm$ for both products in the area [40 - 43 °N ;3 - 8 °E]. A part of the Northern Current flows southwestwards off the Balearic islands.

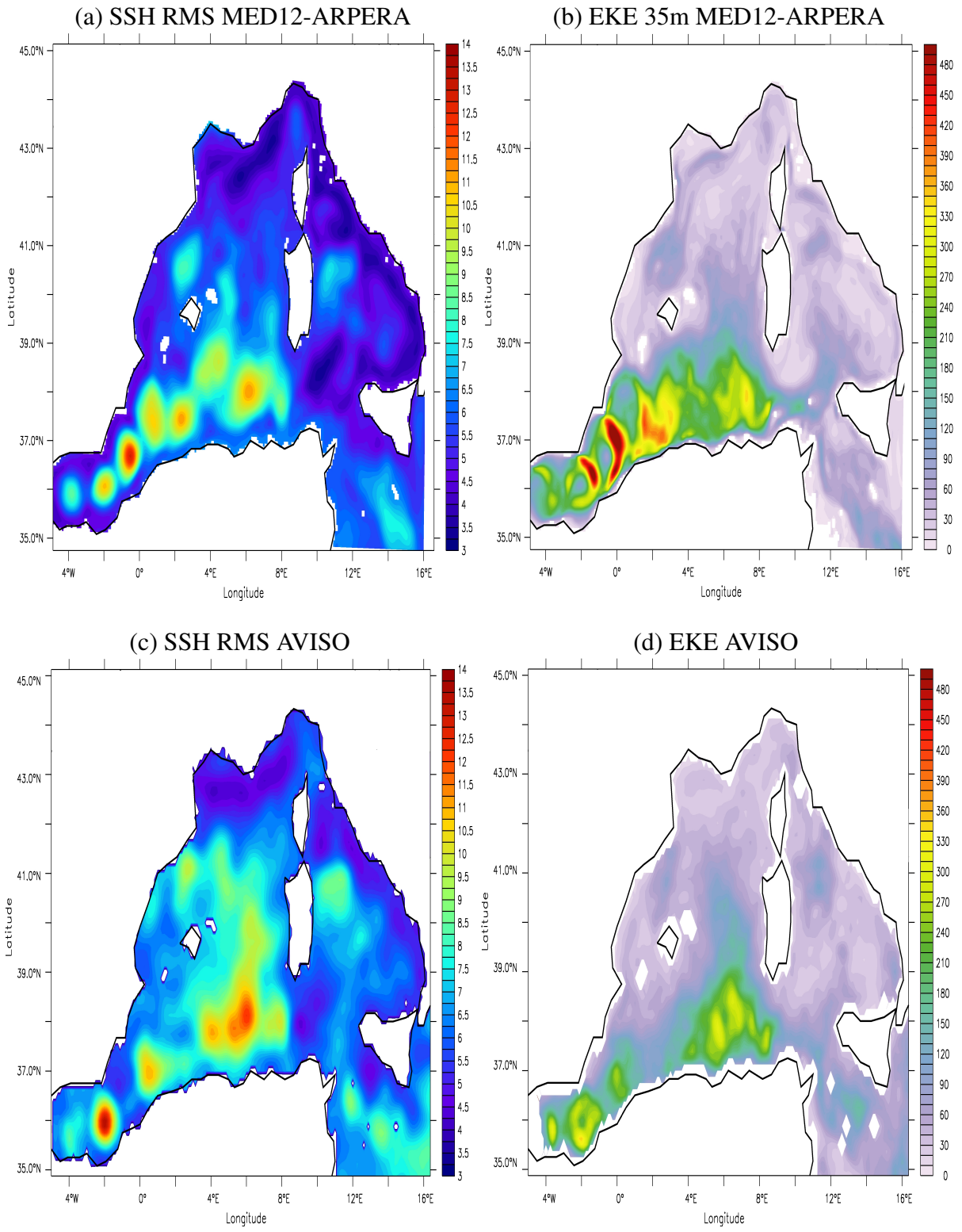

FIG. B.4 – *2004-2008 averages, over the Western Mediterranean, of (left) the RMS of the SSH (SSH Root Mean Square in cm) for (a) MED12-ARPERA and (c) AVISO, and (right) the EKE (Eddy Kinetic Energy in $cm^2.s^{-2}$) for (b) MED12-ARPERA and (d) AVISO. To be consistent with the AVISO geostrophic currents used to calculate the EKE, we took the 35m-depth currents of MED12-ARPERA, i.e. approximately under the mean Ekman layer.*

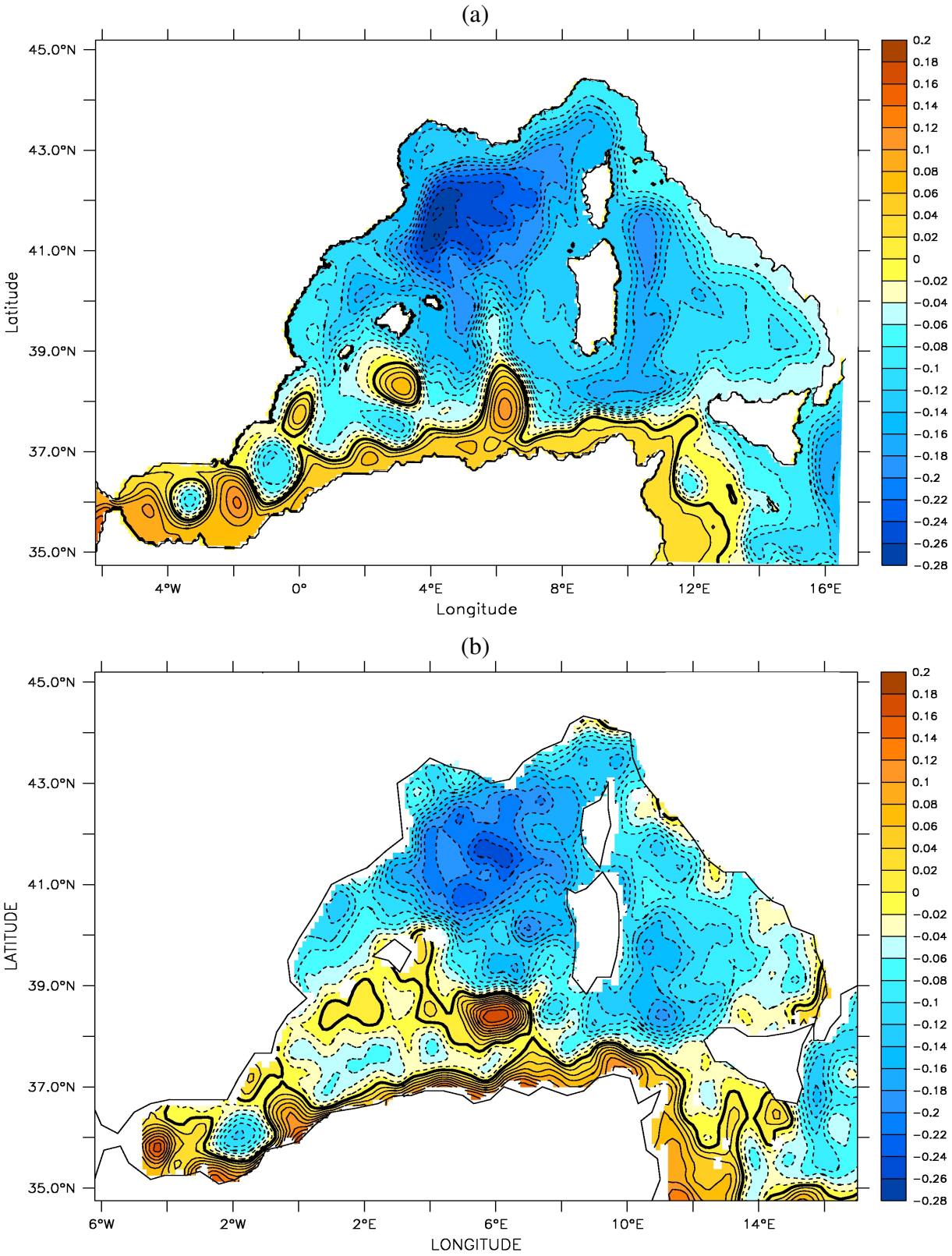

FIG. B.5 – *Monthly mean of the SSH (m) over the Western Mediterranean, for February 2005, (a) for simulation MED12-ARPERA and (b) for AVISO. Contours are every 0.02 m, with dashed lines for negative values (cyclonic) and full lines for positive values (anticyclonic).*

B.3.3 Global and interannual thermohaline characteristics in the Western Mediterranean

To study the representativity of the interannual variability in the simulation in the Western Mediterranean, we analysed the evolution of the SST, SSS, heat and salt contents (Figure B.6), averaged over the Western Mediterranean, $i.e.$ between the Strait of Gibraltar and the Channel of Sicily.

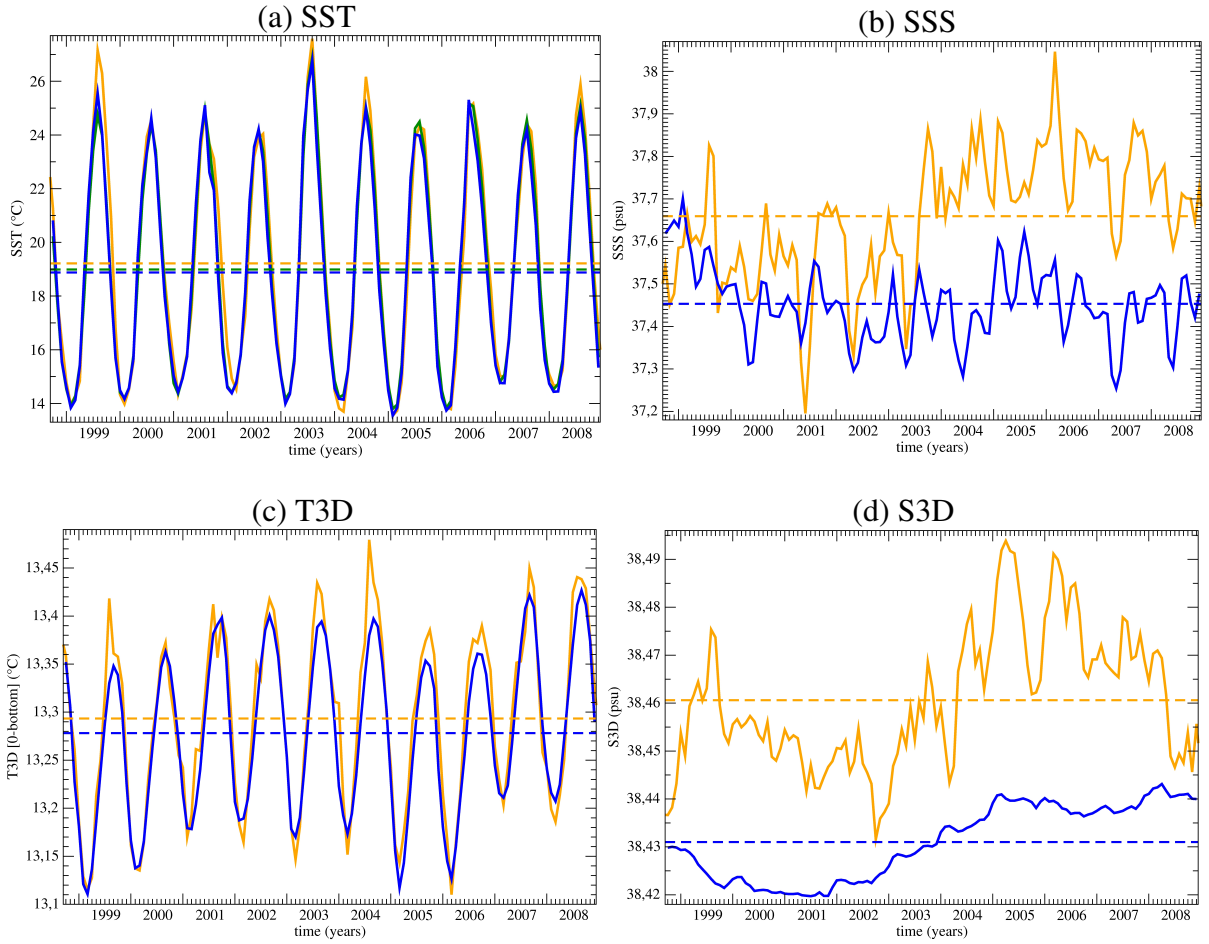

FIG. B.6 – *Monthly time-series, from October 1998 to December 2008, of the* ***Western Mediterranean*** *averages of (a) the sea surface temperature (SST in °C), (b) the sea surface salinity (SSS in psu), (c) the total heat content (shown as a mean potential temperature T3D in °C) and (d) the total salt content (shown as a mean salinity S3D in psu). MED12-ARPERA is in blue, the EN3 dataset (Ingleby and Huddleston, 2007) is in orange and the ERA40/ECMWF SST (Reynolds et al., 2002) is in green. Full lines indicate the monthly values, dashed lines correspond to the averages over the period October 1998 - December 2008.*

For the SST (Figure B.6a), we compare the monthly means of MED12-ARPERA in blue, of the EN3 dataset (*Ingleby and Huddleston*, 2007) in orange and of the ERA40/ECMWF SST (*Reynolds et al.*, 2002) in green. In average over the simulated period, the mean Western Mediterranean SST is 18.88 °C for MED12-ARPERA, 18.99 °C for Reynolds and 19.22 °C for EN3. The monthly variability is very well reproduced in the simulation, thanks to the retroaction term in the forcing heat flux. The interannual variations of the winter minima and summer maxima are also well simulated, except for warm summers in 1999, 2003, 2004 and 2008, during which

MED12-ARPERA SST is slightly lower than EN3 SST.

For the SSS (Figure B.6b), we compare the averages over the Western Mediterranean for MED12-ARPERA (blue) and EN3 (orange). In average over the simulated period, the mean Western Mediterranean SSS is 37.45 psu for MED12-ARPERA and 37.66 psu for EN3. The stability of the SSS over the 10 years of the simulation is obvious, and this is obtained without any sea surface salinity restoring. The monthly SSS variations are in agreement with those of EN3. The sharp SSS increase (jump) in EN3, which can be attributed to the heat wave of summer 2003, is not reproduced in the model and then can explain an important part of the total 10-year bias of MED12-ARPERA SSS in the Western Mediterranean.

For the Western Mediterranean total heat content (given as a mean potential temperature T3D in Figure B.6c), the simulation has a slight cold bias, the mean value over the simulated period being 13.28 °C for MED12-ARPERA (blue line) and 13.29 °C for EN3 (orange line). The seasonnal and interannual variations are well reproduced in the simulation, with a slightly lower amplitude of the monthly cycle than in EN3 (winters less cold and summers less warm in the simulation). In both the simulation and the observed dataset, very cold winters like those of 1999, 2005 and 2006 are identified by the lowest potential temperature values (below 13.15 °C in winter), while other years can be considered as relative warm winters, especially 2007 and 2008, for which the minimum value is higher than 13.2 °C in winter. This alternation of cold and warm winters will be linked further to the occurrence or not of dense water formation in the Gulf of Lions.

For the Western Mediterranean total salt content (given as a mean salinity S3D in Figure B.6d), the simulation has a fresh bias, the mean value over the simulated period being 38.43 psu for MED12-ARPERA (blue line) and 38.46 psu for EN3 (orange line). The simulation shows alternative periods of salinity decrease or increases before and after end-2001, but these variations have a far higher amplitude in EN3. The difference in the amplitude of the monthly variations of S3D between MED12-ARPERA and EN3 can be due to shortcomings in the model, but one has to remind that issues due to undersampling may artificially increase the monthly variations in datasets coming from in-situ observations, espacially for salinity.

Deep convection occurs in the Gulf of Lions during the 10-year period as deduced from the time-series of the daily spatial maximum reached by the convection in the north-western Mediterranean (Figure B.7a). In particular, the convection reaches depths higher than 2000 m depth for events longer than two months in 2000, 2004 and 2006, and longer than one month and a half from end January to early March 2005. We also note that no deep convection occurs in 2007 and 2008 in the simulation. These time-serie is in agreement with another modelling work obtained after a 15-year spin-up (*Béranger et al.*, 2009), showing thus some skills of such short simulations to represent the interannual variability of the general circulation. Looking at the evolution of the volume of dense waters in the north-western Mediterranean (Figure B.7b), we identify the WMDW with the usual density threshold of 29.10 $kg.m^{-3}$, but we also use denser thresholds to highlight the exceptionality of winter 2005 and to better identify the new WMDW. Despite the first two years of spin-up, we can identify that water denser than 29.10 $kg.m^{-3}$ is formed during winters 1999, 2000, 2003, 2004, 2005 and 2006. Water denser than 29.11 $kg.m^{-3}$ is formed during winter 2005 in larger quantities compared to winters 2003, 2004 and 2006. Water denser than 29.12 $kg.m^{-3}$ is only formed, in sizeable amount, during winter 2005. And in early March 2005, water denser than 29.13 $kg.m^{-3}$ is formed (see Table B.2). Thus, the 29.11 $kg.m^{-3}$ can be used in our simulation to characterise the new WMDW and its formation rate in the simulation MED12-ARPERA.

To compare our results with the 2.4 Sv mean estimate over the two winters 2005 and 2006 of *Schroeder et al.* (2008), derived from the volumetric distribution of the θ-S properties in in-situ

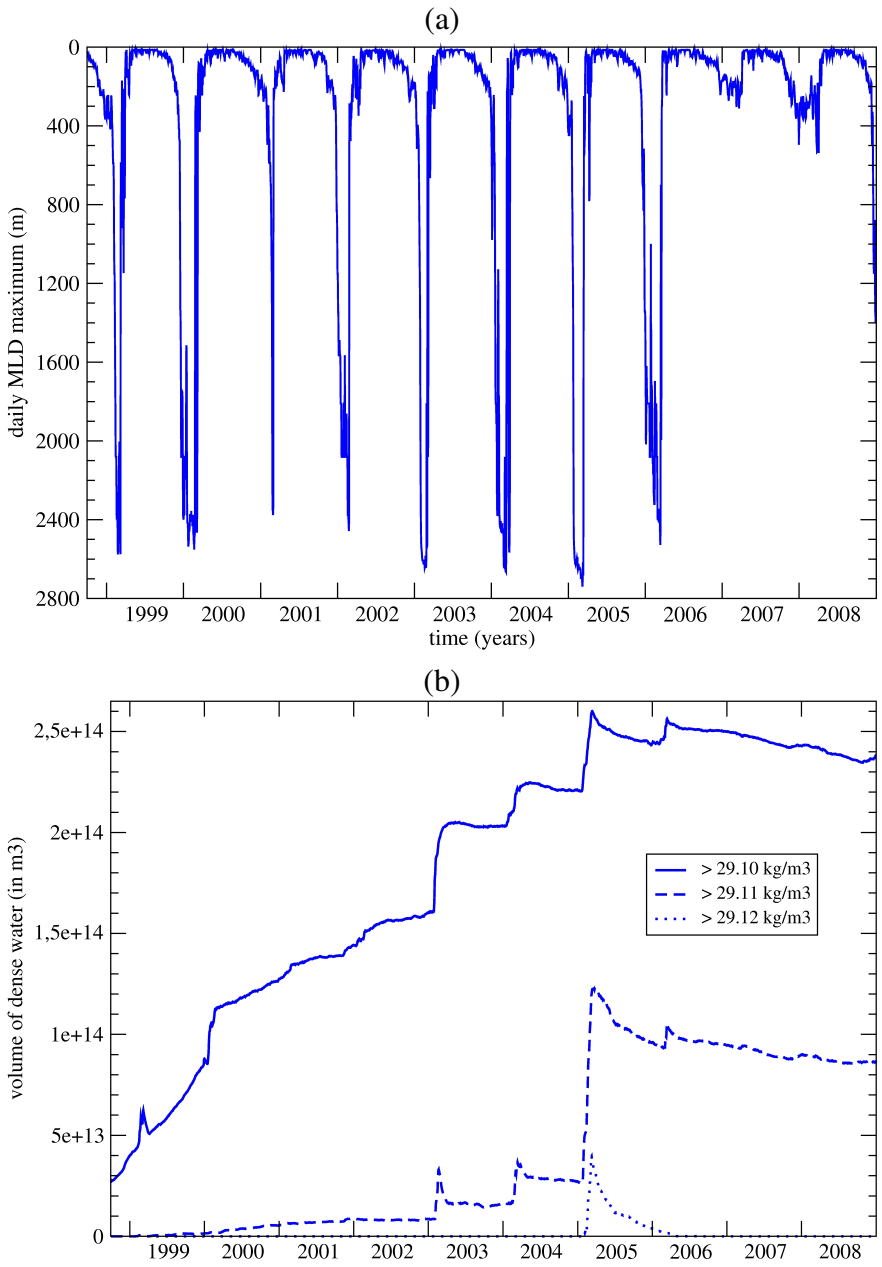

FIG. B.7 – *Daily values, from the 1st October 1998 to the 1st December 2008, of (a) the maximum of the turbocline depth (m) in the north-western Mediterranean (cf. Figure B.1), and (b) the volume (in m^3) of dense waters in the north-western Mediterranean for three thresholds : denser than 29.10 (solid lines), 29.11 (dashed lines) and 29.12 $kg.m^{-3}$ (dotted lines).*

observations for the end 2004 - end 2006 period, we add in Table B.2 the dense water formation rates for winter 2006. With the 29.11 threshold, it gives a mean formation rate over these two winters of 1.73 Sv in the simulation. In comparison, for the single winter 2005, *Béranger et al.* (2009) and *Herrmann et al.* (2010) obtained a formation rate of 1.28 Sv and 1.16 Sv respectively, *i.e.* 2.5 times lower than in MED12-ARPERA (3.05 Sv).

The exceptional winter convection event in 2005 gives the largest volume of dense water formed compared to the 10-year studied period and to other climatological estimates reported

Class / Winter	2005	2006	Mean
$\geq 29.10\,\mathrm{kg.m^{-3}}$	1.26	0.42	0.84
$\geq 29.11\,\mathrm{kg.m^{-3}}$	3.05	0.41	1.73
$\geq 29.12\,\mathrm{kg.m^{-3}}$	1.26	0.00	0.63
$\geq 29.13\,\mathrm{kg.m^{-3}}$	0.28	0	0.14

TAB. B.2 – *Dense water formation rates (in Sv) in the Gulf of Lions for winters 2005 and 2006.*

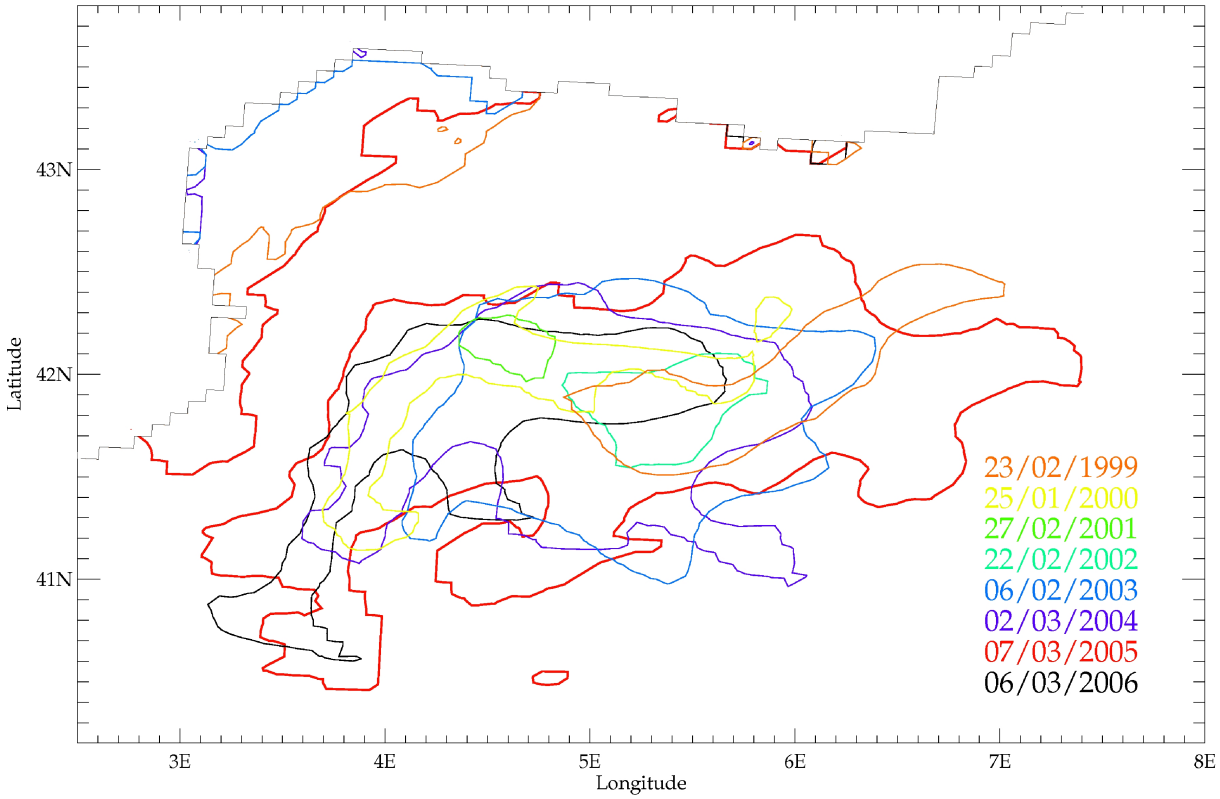

FIG. B.8 – *Daily maximal extent of the 29.10 kg.m^{-3} isopycne at the sea surface in the Gulf of Lions, in winter 1999 (orange, 23rd February 1999), 2000 (yellow, 25th January 2000), 2001 (green, 27th February 2001), 2002 (turquoise, 22nd February 2002), 2003 (blue, 06th February 2003), 2004 (purple, 2nd March 2004), 2005 (red, 7th March 2005) and 2006 (black, 6th March 2006), in simulation MED12-ARPERA-3. In winters 2007 and 2008, the 29.10 kg.m^{-3} isopycne does not reach the sea surface.*

in *Marshall and Schott* (1999). It is also exceptional in terms of spatial extent of the deep convection area. Figure B.8 compares the maximal extent of the 29.10 kg.m^{-3} isopycne outcrop at surface for the 10 winters simulated in MED12-ARPERA (in winters 2007 and 2008, this isopycne does not outcrop). Winter 2005 appears to have the widest convection area (about 48000 km^2, see Table B.3), in the open sea (from the usual location of 42 °N – 5 °E) as on the shelf of the Gulf of Lions. The deep convection area extends south-westwards, downstream of the Northern Current towards the Balearic Islands, but also eastwards until 7.5 °E. Deep mixed layers have been observed in the eastern Catalan subbasin (4.845 °E – 39.785 °N, *Smith et al.* (2008)) in early March 2005. The convection area in MED12-ARPERA, as identified in winter 2005 in Figure B.8, clearly extends to the eastern part of the Catalan subbasin (Csb in Figure B.1), even if it does not reach the far south position observed. During the other winters

Winter	Maximal extent (km^2)
1999	16694
2000	6918
2001	1130
2002	3222
2003	20889
2004	19351
2005	47968
2006	17432
2007	0
2008	0
10-year average and standard deviation	13360 ± 14031

TAB. B.3 – *Maximal extent (in km^2) of the area with sea surface density $\geq 29.10\,kg.m^{-3}$ in the north-western Mediterranean (see Figure B.1 for its boundaries), for the 10 simulated winters in simulation MED12-ARPERA. The average and standard deviation of the 10 yearly maxima are also indicated.*

in this simulation, the convection does not occur in all these parts of the Gulf of Lions, showing again the exceptional intensity of the convection in winter 2005.

For each winter, the day corresponding to the maximal horizontal extent of the $29.10\,kg.m^{-3}$ isopycne outcrop is also indicated in Figure B.8. Winter 2005 has the latest date for this maximal extent, which occurs on the 7^{th} March 2005. It is an other point that underlines the exceptionality of this winter in terms of duration of the severe winter conditions over the Gulf of Lions, well reproduced in the simulation. The occurence of the maximal extent of the convection area in early March is also consistent with surface chlorophyll concentration observations by MODIS satellite reported in *Herrmann et al.* (2010).

B.4 Spreading of WMDW after winter 2005

In this section, we focus on the aim of this study : to characterise, in the simulation, the spreading of the new dense water mass formed in winter 2005, from the convection area in the Gulf of Lions southwards in the Western Mediterranean, and to compare it with in-situ observations made at that time. Then, we adopt successively an eulerian and a lagrangian analysis to estimate the transport time and we discuss about the results we obtain.

B.4.1 θ-S characteristics of the new WMDW

The temperature and salinity characteristics of waters denser than 29.10 in the Gulf of Lions are shown in Figure B.9 for the 1^{st} November 2004, the 7^{th} March 2005, the 1^{st} May 2005 and the 1^{st} November 2005. The densest WMDW at the end of 2004, $i.e.$ before the convection event of 2005, is $29.112\,kg.m^{-3}$ (θ = 12.76-12.78 °C, S = 38.440-38.450 psu, Figure B.9a) ; in comparison, the pre-2005 observed thermohaline characteristics of the WMDW are indicated on Figure B.9a with the black box, showing that the simulation starts this winter with the good deep water characteristics in the Gulf of Lions. During the most intense phase of

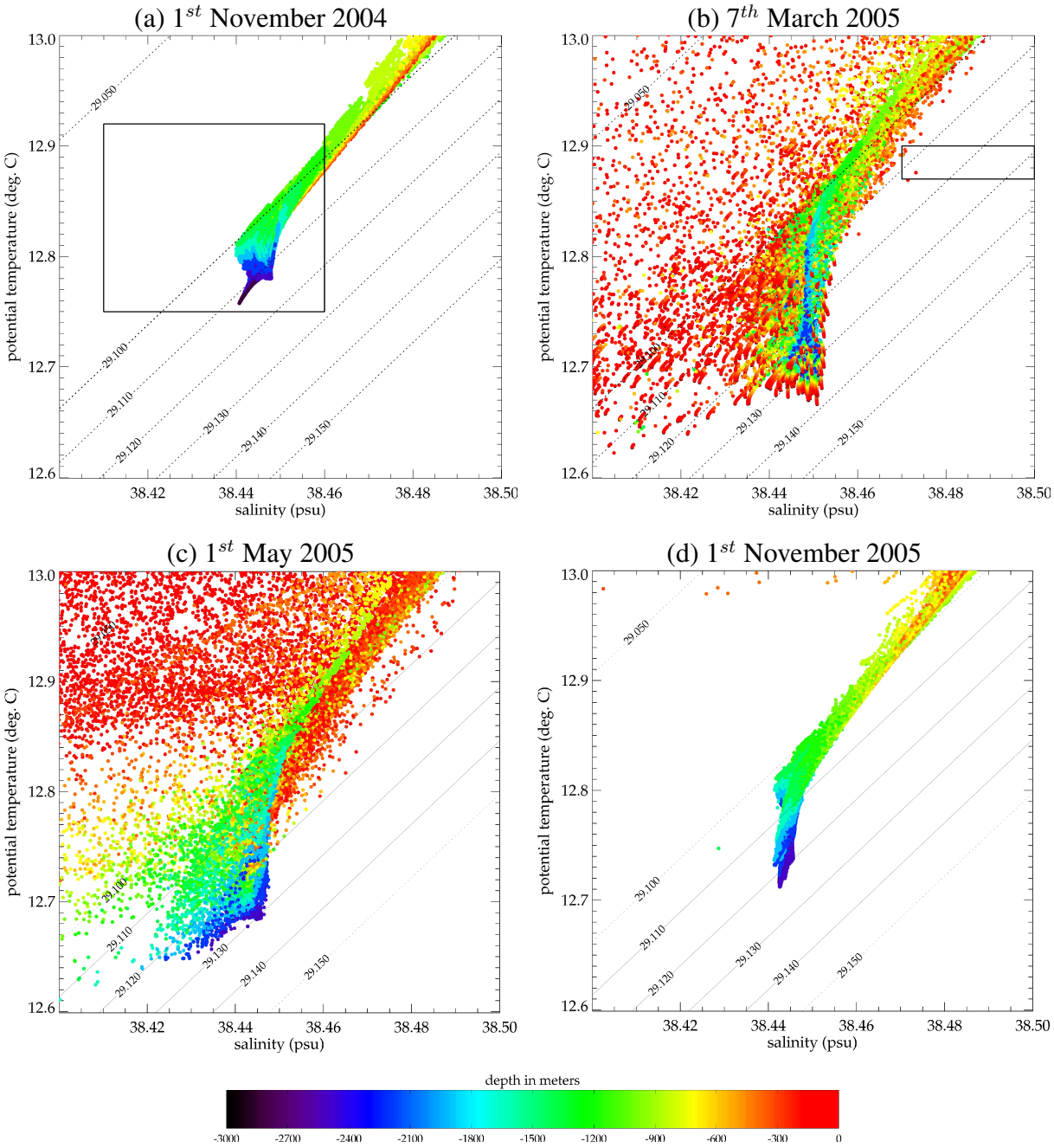

FIG. B.9 – *θ-S diagrams in the Gulf of Lions, in simulation MED12-ARPERA-3, for (a) the 1st November 2004, (b) the 7th March 2005, (c) the 1st May 2005 and (d) the 1st November 2005. The color of the dots indicates the depth in the model. Thin and dashed lines indicate potential density values in kg.m^{-3}. The box in figure a (resp. b) indicates the pre-2005 (resp. 2005) thermohaline characteristics of the WMDW found in the literature.*

the deep convection event, the 7th March 2005 in the simulation, the new WMDW is characterised by a maximal density of 29.138 kg.m^{-3} (θ = 12.67-12.72 °C, S = 38.440-38.453 psu, Figure B.9b). Two months later in spring, after the restratification phase, this highest density is still above 29.130 kg.m^{-3} (θ = 12.65-12.71 °C, S = 38.435-38.448 psu, Figure B.9c) whereas eight months later it has decreased by about 0.01 kg.m^{-3} in the Gulf of Lion towards 29.123 kg.m^{-3} (θ = 12.70-12.75 °C, S = 38.442-38.448 psu, Figure B.9d). Compared to observations of *López-Jurado et al.* (2005), *Schröder et al.* (2006), *Font et al.* (2007) and *Smith et al.* (2008), who

reported $\theta = 12.87\text{-}12.90\,^{\circ}\mathrm{C}$ and $S = 38.47\text{-}38.49$ psu (black box in Figure B.9b), the thermohaline characteristics of the new WMDW formed in winter 2005 in the model are not warm enough and not salty enough. Obtaining such an agreement is very difficult with a numerical model, mainly because of uncertainties in the initial conditions, the atmospheric fluxes and the physics of the model. Here, it could be related to the presence or not of dense water formed during the Eastern Mediterranean Transient in the early 1990's (*Roether et al.*, 2007) in the simulation or in the initial conditions only. In fact, *Herrmann et al.* (2010) obtained more accurate θ-S characteristics for the new WMDW with the same ARPERA atmospheric forcing but within a 46-year simulation, containing thus a well simulated EMT and not only an EMT hardly present in the initial state of the simulation, as we do. Nevertheless, the density signature is in agreement with observations in our simulation, allowing us to follow the deep water mass propagation in the model.

B.4.2 θ-S characteristics in the South of the Western Mediterranean

Following the observations of *Schroeder et al.* (2008), we look at the thermohaline characteristics of waters near the Channel of Sardinia and the Strait of Gibraltar to detect the arrival of the new WMDW at these places. Even if our results are satisfying for the Channel of Sardinia, the model does not succeed in catching such signature at the Strait of Gibraltar. We consider then the θ-S diagram of waters in two boxes (see Figure B.1), box 1 west of the Channel of Sardinia [8 °E ; 9 °E]-[37 °N ; 39 °N], and box 2 west of the Algerian subbasin [2 °E ; 3 °E]-[36.5 °N ; 39 °N]. In the two boxes, the last point of the θ-S diagrams corresponds to 2530 m depth.

For the Sardinian area (Figure B.10a), there is no change in the deep thermohaline characteristics between the 1^{st}October 2004 (black line) and the 1^{st} December 2005 (dark blue line). A noticeable change starts to appear during December 2005, since the profile of the 1^{st} January 2006 (light blue line) shows waters slightly denser, colder and saltier than the previous one. Then, these changes continue in the same way and for the 1^{st} October 2006 (red line) the deep water has become denser by $0.002\,\mathrm{kg.m^{-3}}$ ($\rho = 29.113\,\mathrm{kg.m^{-3}}$), colder by 0.005°C ($\theta = 12.758$°C) and saltier by 0.001 psu ($S = 38.442$ psu) than before. Thus, in the model, it takes about 9 to 10 months (from February-March to December 2005) for the new WMDW to reach the Channel of Sardinia. The signature of this new water mass is relatively weak because the density of old water is initially of 29.111 at this place, which is relatively high but which corresponds to the density of the old WMDW in the Gulf of Lions (as seen in section B.4.1). Nevertheless, reminding that it is obtained for very deep water and by averaging over a box of $1^{\circ} \times 2^{\circ}$, this signature is noticeable.

For the Algerian area (Figure B.10b), between the 1^{st} October 2004 (black line) and the 1^{st} January 2006 (dark blue line), the slight deep warming and salting associated with a tiny density decrease are certainly caused by mixing or diffusion with water above and not by the advection of a new water mass, since the new WMDW are colder and denser than the old one. Then, the deep thermohaline characteristics of this area remain almost constant until the 1^{st} March 2006 (light blue line). A significant change starts to appear during March 2006, since the profile of the 1^{st} April 2006 (green line) shows waters slightly colder and denser than the previous one. Then, the profile for the the 1^{st} October 2006 (red line) is denser, coldier and saltier than 9 months before, changes and new characteristics being similar as those of the Sardinian area. Thus, in the model, it takes about 12 to 13 months (from February-March 2005 to March 2006) for the new WMDW to reach the deep area between the Balearic islands and the Algerian coast.

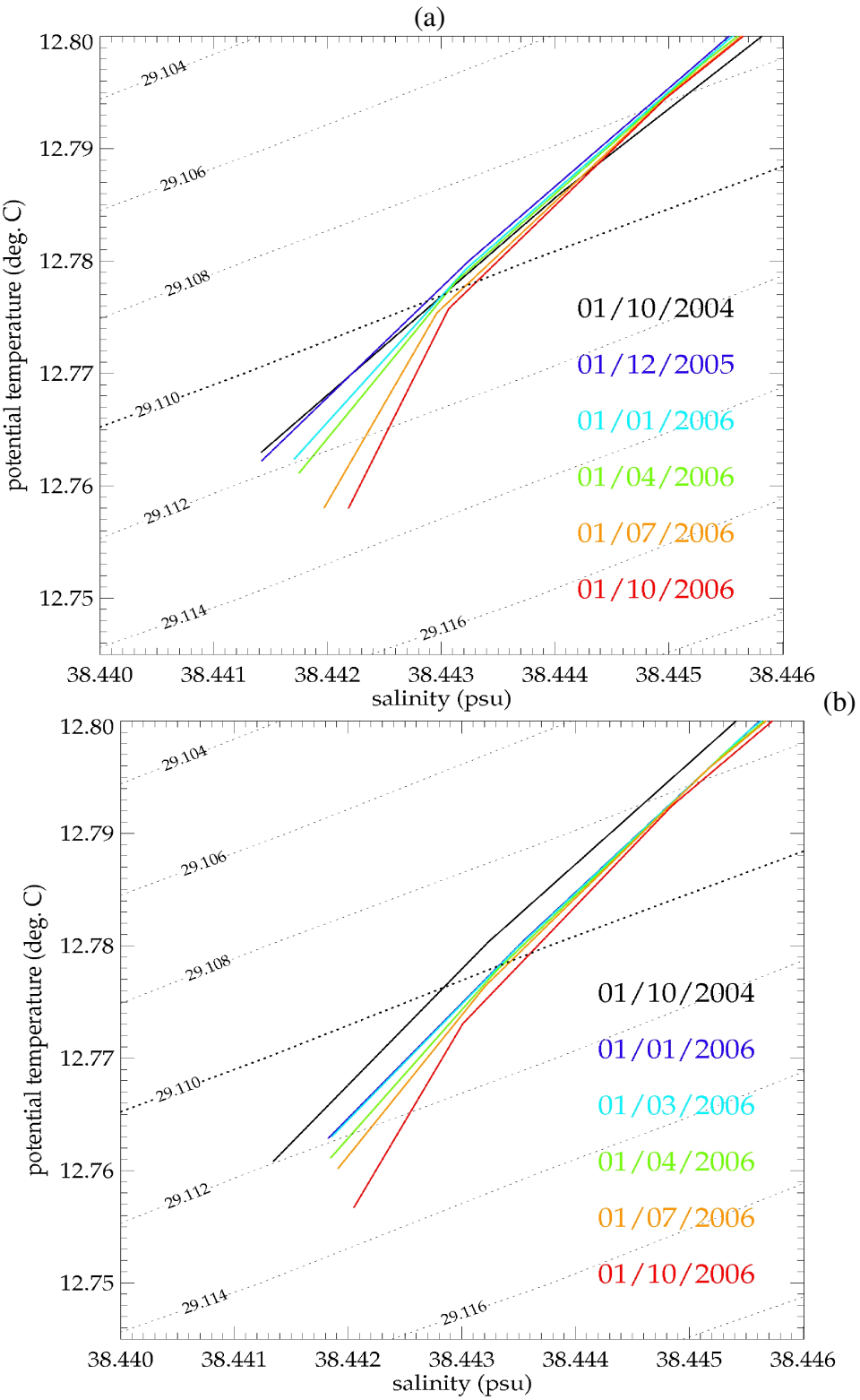

FIG. B.10 – *Bottom end of θ-S profiles averaged (a) over the box [8°E ; 9°E]-[37°N ; 39°N] (box 1 in Figure B.1, west of the Channel of Sardinia) and (b) over the box [2°E ; 3°E]-[36.5°N ; 39°N] (box 2 in Figure B.1, west of the Algerian subbasin), in simulation MED12-ARPERA. Dashed lines indicate potential density values in kg.m^{-3}. The correspondance between dates and colors is indicated within the diagram.*

B.4.3 Transport estimates

B.4.3.1 Eulerian considerations

Using the results of the simulation MED12-ARPERA, we follow the deep spreading of the new WMDW formed in winter 2005. As argued in section B.3.3, the core of the new WMDW in the model is identified by the 29.11 kg.m^{-3} threshold. The depth of the $\sigma_0 = 29.11$ isopycne (Figure B.11) is a first way to follow the propagation of the new WMDW. To favour the comparison with observations, we choose the same dates as in *Schroeder et al.* (2008). In October 2004 (Figure B.11a), the preconditionning due to the cyclonic gyre in the Gulf of Lions is obvious, inducing a doming of the isopycnal surfaces and thus the 29.11 isopycne depth is less than 1600 m in this area. In the other part of the Algero-Provencal subbasin, the isopycnal surface is deeper than 2100 m, and even deeper than 2500 m near the Ligurian subbasin (Lsb in Figure B.1). There is no water with such a density or denser in the Catalan subbasin (Csb in Figure B.1) and in the center of the Ligurian subbasin. In June 2005 (Figure B.11b), $i.e.$ 3 months after the end of the deep convection event, the core of the recently formed water mass is located between the Gulf of Lions and the Balearic Islands, and the 29.11 isopycne is shallower than 500 m. New WMDW is present in the eastern part of the Catalan subbasin (in consistence with the occurence of deep convection in this area, as described in Figure B.8) and flows along the continental slope off the coast of Minorca Island (easternmost island of the Balearic archipelago). From the convection area, the new WMDW spreads also to the east towards the center of the subbasin. In October 2006 (Figure B.11c), the 29.11 isopycne is located at lower depth in the northwestern part of the subbasin, because of the steady cyclonic circulation. But it is obvious that in all the Western Mediterranean, the isopycnal surface has been uplifted, compared with the ocean state two years before. This uplift is of the order of about 200 m in the area between the Algerian coast and the Balearic Islands, with higher differences along the Balearic continental slope. The uplift amounts to 400 m in the center of the cyclonic gyre of the Gulf of Lions (from less than 1600 m in October 2004 to less than 1200 m in October 2006). The uplift is the most substantial in the Ligurian subbasin, in which the depth of the 29.11 isopycne varies from 2700 m in October 2004 to about 1800 m in October 2006. This is in good agreement with *Schroeder et al.* (2008), who evidenced an uplift of the $\sigma_{1000} = 33.477$ isopycne of about 100-150 m in the southern part of the subbasin and 200 m in the northern part, up to 1000 m in the Ligurian subbasin.

Figure B.12 shows the potential density and the horizontal current at 2225 m depth for different days from mid-June to end-December 2005. In June 2005 (Figure B.12a), $i.e.$ 3 months after the end of the deep convection event, the densest waters have started to exit the former convection area (around 42 °N – 5 °E) and flow southwards along the slope of the Balearic Islands between 42 °N and 40 °N ; the potential density is still high (≥ 29.125 kg.m^{-3}). A cyclone, identified by C1 in Figure B.12a, starts to trap dense water and to carry it quicker southwards. The separation of the cyclone from the core of the dense water flow seems to be made easier by a northwestwards intrusion of light water, obvious around 41 °N – 5 °E. About one month later in early August 2005 (Figure B.12b), the cyclone C1 is well defined, around 39 °N – 5.5 °E, with a density gradient higher than 0.01 kg.m^{-3} between the center and the surrounding of the cyclone. It has an horizontal extent of about $1.5° \times 1°$, with an elliptic shape. A second cyclone, identified by C2 in Figure B.12b, starts to form within the densest part of the water mass (near 40.5 °N – 4.5 °E). At the end of August 2005 (Figure B.12c), C1 is now located between 38 °N and 39 °N, while C2 starts to move southwards, still along the continental slope of the Balearic Islands. At the end of October 2005 (Figure B.12d), the signature of C1 is less obvious, while C2 is separating from the flow of the densest water mass. Again, an intrusion of light water occurs simultaneously with the separation of the cyclone C2. In early December 2005 (Figure B.12e),

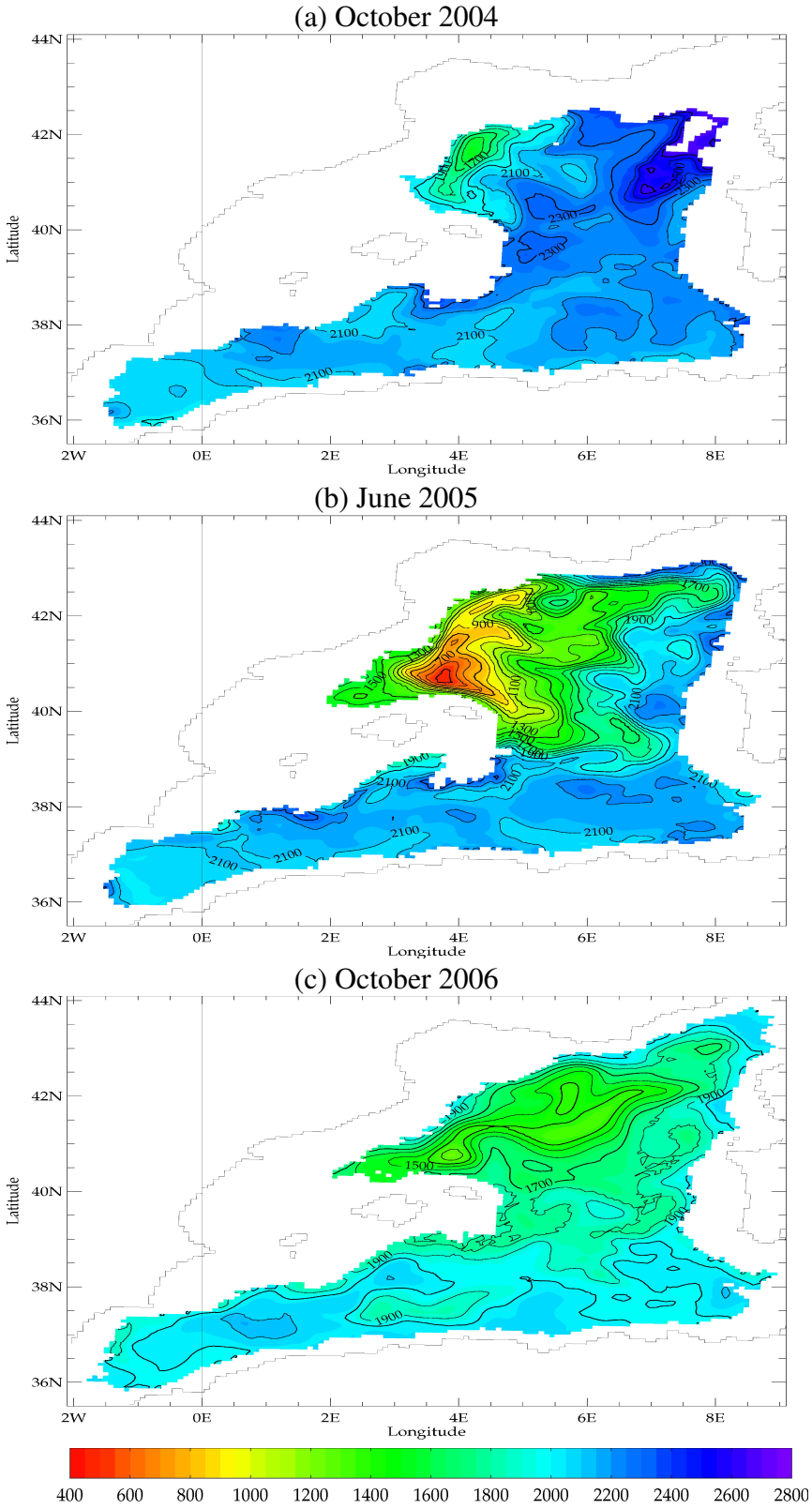

FIG. B.11 – *Monthly averages of the depth (in meters, contour lines every 100 m) of the $\sigma_0 = 29.11$ isopycnal surface, for (a) October 2004, (b) June 2005 and (c) October 2006.*

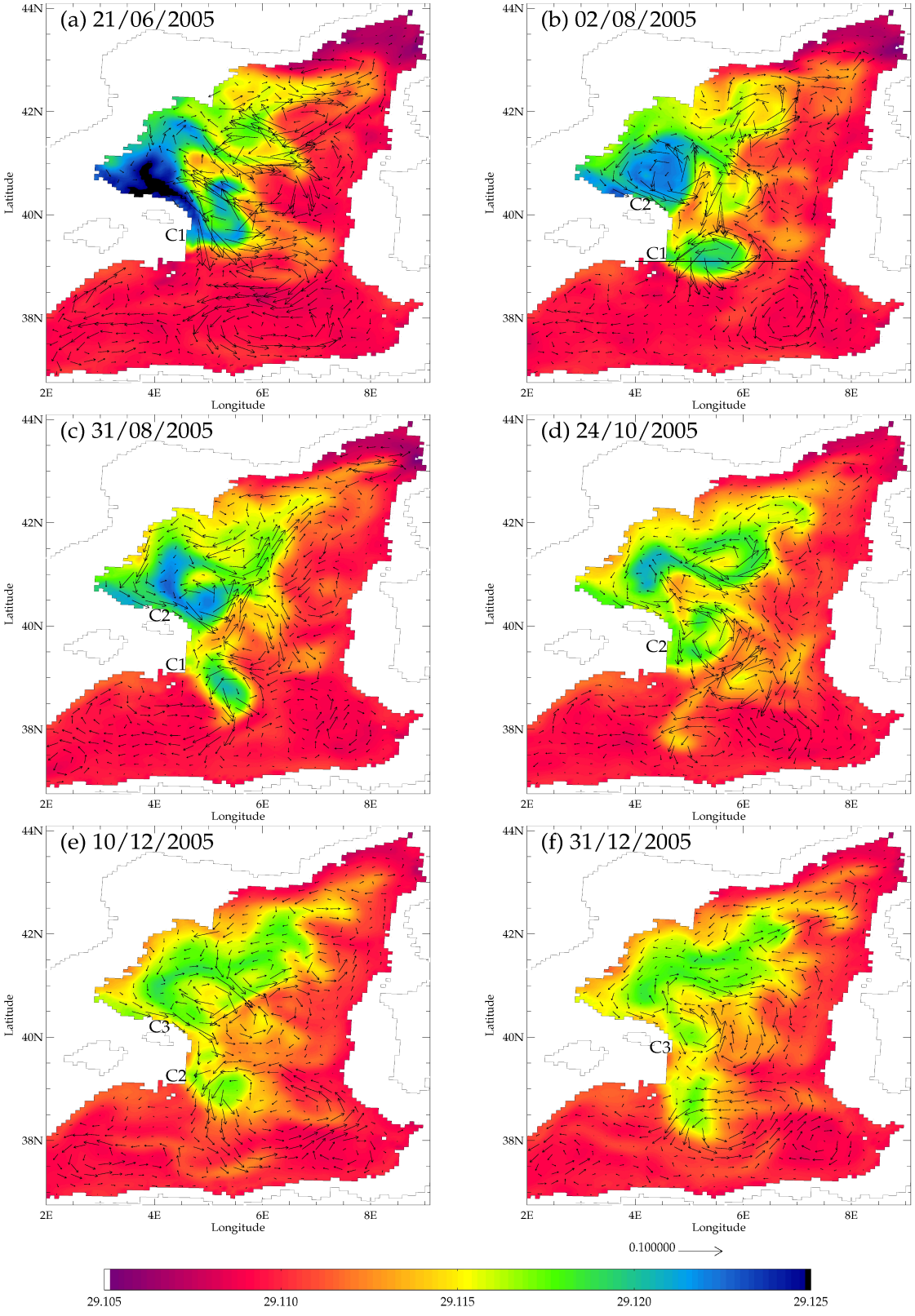

FIG. B.12 – *Potential density (colors, in kg.m^{-3}) and currents (arrows, in m.s^{-1}), at 2225m depth, for (a) the 21st June 2005, (b) the 2nd August 2005, (c) the 31st August 2005, (d) the 24th October 2005, (e) the 10th December 2005 and (f) the 31st December 2005. One vector in three is plotted. C1 ,C2 and C3 identify the three successive deep cyclones. The section of Figure B.13 is drawn on map (b).*

C2 can be identified at about 39 °N, with an horizontal extent of about $1° \times 1°$ and a more circular shape than C1. A third cyclonic eddy, named C3, starts to appear near 40.5 °N – 4.5 °E. At the end of December 2005 (Figure B.12f), C3 crosses the 40 °N line and C2 is not identifiable anymore, even if the dense water mass signature which was previously associated with it ($\rho \geq 29.115$ kg.m^{-3}) is still noticeable at 5 °E and between 38 °N and 39 °N. At the end of December 2005, the deep circulation in the Algerian subbasin is more constrained by the cyclonic eastern Algerian gyre (identified by *Testor et al.* (2005b)) than for previous dates.

A vertical section through the cyclone C1 at the date of Figure B.12b (early August 2005) enables to define the vertical signature of this eddy. Figure B.13a shows the meridian speed and the potential density across C1. A maximum meridian speed of 24 cm.s^{-1} is reached at the surface. It is obvious that C1 is barotropic since it has a vertical extent from the bottom to the surface of the sea. It induces a doming of the isopycnal surfaces, particularly noticeable below the stratified summer surface layer. The layer of water denser than 29.11 kg.m^{-3} is about 1500 m thick in the center of the cyclone, with a weak vertical stratification. Inside C1, below 700 m depth, θ ranges between 12.71 and 12.85 °C and S ranges between 38.44 and 38.45 psu (Figure B.13b). This corresponds well with the values found in the Gulf of Lions during and after the convection event in the simulation. Again, it highlights that the new WMDW in the model is not warm enough and not salty enough compared to in-situ observations made at that time. Around C1, the warm and salty LIW layer is well identifiable, with a core at about 400 m depth ($\theta \geq 13.40$ °C, S ≥ 38.55 psu). The vertical doming induced by C1 is also noticeable for the isothermal and isohaline surfaces (Figure B.13b).

We have shown with Figure B.13 that C1 is a barotropic cyclone. So are C2 and C3 (not shown). Thus, their signature in terms of currents can be seen until the sea surface. The Sea Surface Height (SSH) of the model can be used to follow the paths of these cyclonic eddies (Figure B.14). The comparison between the SSH and the Barotropic Stream Function (BSF, Figure B.15) allows to distinguish, among the surface eddies identifiable with the SSH, those which are barotropic and which thus carry water throughout the whole water column. Figure B.15 shows the same dates as Figure B.12 and B.14 to easily identify the same cyclones C1, C2 and C3. From June 2005 to December 2005, the cyclonic eddies previously identified have the highest values of BSF in the center of the Algero-Provencal subbasin. About 15 Sv of water over the whole column are carried southwards by C1 in June 2005 (Figure B.15a), at most 10 Sv are carried southwards by C2 (Figure B.15b) and at most 7 Sv are carried southwards by C3 (Figure B.15e). In terms of SSH (Figure B.14), the three successive barotropic cyclones have a surface signature and move southwards off the coast of Minorca, from 40 °N to 38 °N, between 5 °E and 6 °E. In the model, the southwards propagation of these three successive cyclones lasts more than 6 months, from June 2005 to December 2005.

A comparison with an observed SSH could assess if the eddies identified by the SSH of the model are realistic, and thus if the occurence of deep barotropic cyclones during summer 2005 is credible. Here again, we use the weekly MADTs of AVISO (Figure B.16). In the observations, two cyclones, CA and CB, propagate successively southwards off the coast of Minorca between early-June 2005 (Figure B.16a) and early August 2005 (Figure B.16e). At the end of August 2005, no cyclonic eddy is noticeable in the area of interest (not shown). They are located around 5 °E, whereas in the model C1, C2 and C3 are around 5.5 °E. Nevertheless, the occurence of cyclonic eddies propagating southeastwards then southwards near 40 °N – 5 °E is realistic and confirmed by satellite observations. The time transport of these eddies is estimated at about 2 months. It is about 4 months shorter than in the simulation MED12-ARPERA. This slower propagation in the model could be explained by a fewer volume of dense water formed in the model than in reality, which could hinder the spreading of dense water. The vertical resolution

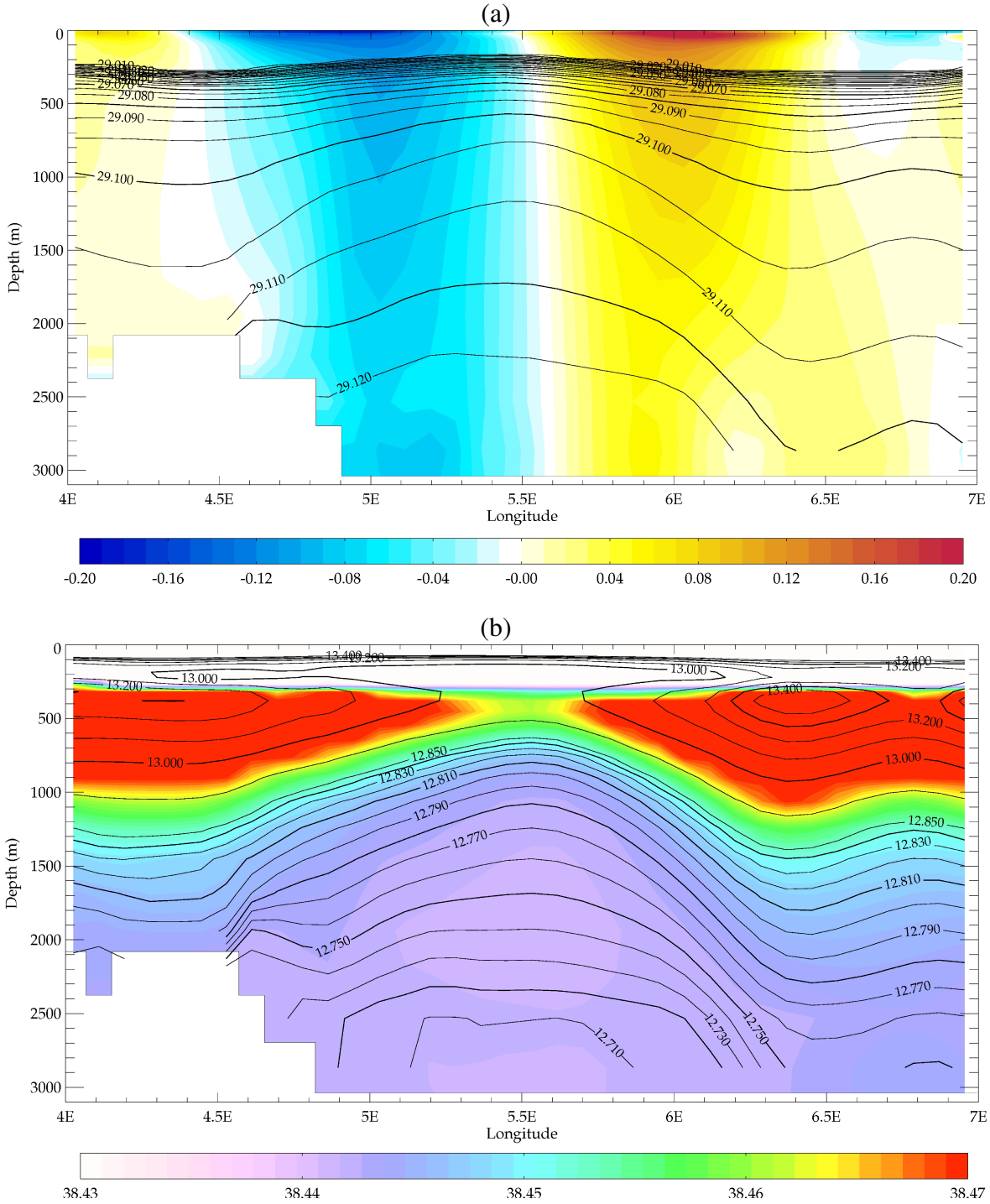

FIG. B.13 – *Vertical sections at 39.1 °N through cyclone C1, in simulation MED12-ARPERA-3 for the 2nd August 2005. (a) Meridian speed (colors, in m.s^{-1}, negative values for southwards current, positive values for northwards current) and potential density (in kg.m^{-3}, contour lines from 29.00 kg.m^{-3} every 0.005 kg.m^{-3}). (b) Salinity (colors, in psu) and potential temperature (in °C, contour lines every 0.01 °C up to 12.85 °C, then every 0.1 °C from 12.9 °C to 13.5 °C).*